Determinants of visual function and progression of retinal pigment epithelium atrophy in late age-related macular degeneration

Habilitationsschrift zur Erlangung der Lehrbefugnis
der Hohen Medizinischen Fakultät
der Rheinischen Friedrich-Wilhelms-Universität
Bonn

Dr. med. Maximilian Pfau

15.11.2020

Dedication

This thesis is dedicated to my mother, Britta Pfau. *Thank you for raising me, for supporting me throughout my life and for providing the initial impetus for my interest in natural sciences through countless visits to 'Technikmuseen' and your support for my participation in pre-college science competitions.*

Contents

List of Abbreviations

ARMS2 age-related maculopathy susceptibility 2. 10, 47

C3 complement component 3. 47

CFH complement factor H. 10

HTRA1 HtrA serine peptidase 1. 10

RHO rhodopsin. 50

AMD age-related macular degeneration. 3, 9–14, 16–18, 29, 32, 36, 44, 45, 47, 50, 51

anti-VEGF anti-Vascular Endothelial Growth Factor. 10, 48

apo apolipoprotein. 11

AREDS age-related eye disease study. 10, 47

BCVA best-corrected visual acuity. 9, 10, 12, 14, 21

BLamD basal laminar deposit. 43

BLinD basal linear deposit. 11

BrM Bruch's membrane. 11, 14, 17, 47–50, 53

CC choriocapillaris. 10–12, 17, 43, 47–49, 51, 53

CFP color fundus photography. 14

cRORA complete retinal pigment epithelium and outer retinal atrophy. 33

cSLO confocal scanning laser ophthalmoscopy. 12, 21

DA Dark adapted. 29–32, 34–38, 43–46, 49, 50, 52

DSGA Directional Spread in Geographic Atrophy. 21, 42

EC esterified cholesterol. 11

ELM external limiting membrane. 12, 23, 33

ETDRS Early Treatment Diabetic Retinopathy Study. 21

EZ ellipsoid zone. 23

FA fluorescein angiography. 42

FAF fundus autofluorescence. 12, 13, 15, 17, 18, 21–23, 27, 39, 40, 51, 52

FAM Fundus Autofluorescence imaging in Age-related Macular degeneration. 21, 47

FCP fundus-controlled perimetry (a.k.a. microperimetry). 15, 18, 21, 23, 24, 49, 52

GA geographic atrophy. 10, 12, 13, 15, 16, 18, 21–27, 29–33, 35, 36, 39–41, 43–47, 49–53

HFL Henle's fiber layer. 23, 44, 45

HFL+ONL Henle's fiber layer and outer nuclear layer. 12, 16, 23, 33–35, 37, 38, 44, 45, 51, 52

ILM internal limiting membrane. 23

IncMSE increase in mean squared error. 37, 38

INL inner nuclear layer. 33–35

IQR interquartile range. 30

IR infrared reflectance. 12, 15, 21, 22, 24

IS photoreceptor inner segments. 23, 45

MAC membrane attack complex. 11

MAE mean absolute error. 36, 49

MNV macular neovascularization. 4, 13, 14, 17, 23–25, 27, 28, 41–43, 47–49, 53

OCTA Optical Coherence Tomography Angiography. 14, 21, 23, 24, 42, 49, 51

ONL outer nuclear layer. 23, 43, 45

OPL outer plexiform layer. 23, 33–35

ORT outer retinal tubulation. 33, 35

ORTs outer retinal tubulations. 33–35, 44, 49, 52

OS photoreceptor outer segments. 23, 45

RPD reticular pseudodrusen (subretinal drusenoid deposits). 9, 11, 17, 23, 44

RPE retinal pigment epithelium. 4, 9–18, 21, 23–25, 27, 28, 33, 41–45, 47–49, 51–53

RPEDC retinal pigment epithelium-drusen complex. 23, 37

SD-OCT Spectral Domain Optical Coherence Tomography. 11, 12, 14, 15, 18, 21, 23, 24, 26, 34–37, 42, 45, 46

SNPs single nucleotide polymorphisms. 10

VEGF Vascular Endothelial Growth Factor. 15

Chapter 1

Introduction

1.1 Age-related Macular Degeneration

Age-related macular degeneration (AMD) constitutes the leading causes of legal blindness in industrialized countries (Colijn et al., 2017; Lim et al., 2012).

The **epidemiology** of AMD is characterized by a drastically increasing prevalence of early and late AMD after the age of 75 years (Wong et al., 2014). According to a meta-analysis by the *European Eye Epidemiology (E3)* consortium, the prevalence of early and late AMD increase from 3.5% and 0.1% in those aged 55-59 years to 17.6% and 9.8% in those aged 85 years or older (Colijn et al., 2017), which makes age the strongest non-modifiable risk factor. Further important non-modifiable risk factors include being of white European descent (compared with individuals of Asian, African, or Hispanic descent), family history and/or genetics (Colijn et al., 2017; R. Klein et al., 2006; Wong et al., 2014). Specifically, genetic risk can be attributed to single nucleotide polymorphisms in complement associated genes and variants on chromosome 10q26 (Fritsche et al., 2014). Smoking constitutes a major modifiable risk factors (2 to 4-fold increase in prevalence across all stages) (Smith et al., 2001). Other modifiable risk factors include diet (low in carotenoids and/or other antioxidants, or high in fat) (Merle et al., 2019), hypertension (R. Klein et al., 2003), high-density lipoprotein (HDL) cholosterol (Colijn et al., 2019), and possibly the lack of physical activity (McGuinness et al., 2017).

The **clinical course** of AMD is hallmarked by formation of extracellular subretinal pigment epithelium (RPE) deposits in the macula termed soft drusen, which are readily visible in funduscopy (Curcio, 2018b). Other initial, although disease-unspecific, lesions include reticular pseudodrusen (subretinal drusenoid deposits) (RPD) and hyperpigmentary changes (Curcio, 2018b). The presence and extent of these three above listed lesions are marked intraocular risk factors for the progression of intermediate AMD to late AMD. Typically, patients with early and intermediate AMD are asymptomatic, but these patients may also experience impaired night vision, contrast sensitivity and metamorphopsia. Late AMD is defined by evidence of current or former exudation secondary to neovascularization and/or RPE atrophy. Exudation typically leads to marked metamorphopsia and will result - if untreated - in an average loss of best-corrected visual acuity (BCVA) of 3 lines in two years (Rosenfeld et al., 2006). RPE atrophy in non-exudative late AMD results in absolute scotoma. Typically, these foci of atrophy spare the fovea initially resulting

in paracentral loss of vision and reading impairment. Foveal involvement over time results in a corresponding loss of BCVA (Lindner et al., 2019; Sunness et al., 2008).

Established treatments include the combined oral supplementation of antioxidants, xanthophylls, copper and zinc as ingredients of the so-called age-related eye disease study (AREDS) formulation and anti-Vascular Endothelial Growth Factor (anti-VEGF) therapy (Lim et al., 2012). Specifically, the age-related eye disease study (AREDS) formulation (vitamins C and E, beta carotene, copper and zinc) and AREDS 2 formulation (vitamins C and E, lutein, zeaxanthin, copper and zinc) were shown to decrease the probability of progression from (high-risk) intermediate to late AMD (Chew et al., 2013; Kassoff et al., 2001). However, the effect is mostly driven by a reduced probability of progression to neovascular AMD (Chew et al., 2013; Kassoff et al., 2001). Today, exudation secondary to neovascularization in AMD may be effectively treated by anti-VEGF therapy for 24 months and longer (Rosenfeld et al., 2006). But the long-term results of anti-VEGF monotherapy are less favorable with a loss of best-corrected visual acuity (BCVA) of three lines or more in a third of patients (Rofagha et al., 2013). No treatment is available for the degenerative component of the disease in the setting of GA as well as for fibrotic scarring secondary to exudation (Lim et al., 2012). Last, it was shown that short-term, high-dose retinol supplementation modestly improves the rate of rod-mediated dark adaptation in patients with early to intermediate AMD (Owsley et al., 2006).

1.2 Underlying Disease Biology

The underlying biology of the disease is incompletely understood. AMD is a complex, multi-factorial disease. However, two chromosomal regions were consistently shown to be associated with risk of AMD progression across disease stages: (i) one on chromosome 1 (1q32), which includes SNPs in complement factor H (*CFH*) (Edwards et al., 2005; Hageman et al., 2005; Haines et al., 2005; R. J. Klein et al., 2005), and (ii) one on chromosome 10 (10q26) harboring two genes, namely age-related maculopathy susceptibility 2 (*ARMS2*) and HtrA serine peptidase 1 (*HTRA1*) (Jakobsdottir et al., 2005; Rivera et al., 2005). While the association of complement factor H (*CFH*) genotype with AMD is partially understood (cf. below), the precise relationship of the *ARMS2/HTRA1* region with AMD remains unclear. Since the *ARMS2/HTRA1* region on chromosome 10 displays correlated variants in high linkage disequilibrium, it is controversial to which gene the observed AMD risk can be attributed to. Analysis of rare recombinant haplotypes by the *International AMD Genomics Consortium* identified variants in *ARMS2* exclusively as carriers of the AMD risk (Grassmann et al., 2017). However, the function of the gene product remains unclear. In contrast, expression of *HTRA1* in the RPE, horizontal cells and macroglia (Müller glia and astrocytes) could be evidenced (Menon et al., 2019). Recently, an anti-HtrA1 Fab to inhibit HtrA1 proteolytic activity has been developed and is currently probed clinical studies aiming to slow GA progression (Tom et al., 2020). The results of this trial will likely refine the understanding of the role of HtrA1 in AMD (Tom et al., 2020).

Pre-clinical, early and intermediate AMD is characterized by **impaired interchange** between the choriocapillaris (CC) and the RPE, which has been attributed mainly to two pathways. First, genetic risk at the *CFH* locus as well as smoking were shown to be associated with complement activation at the human

RPE-choroid interface (Keenan et al., 2015; Mullins et al., 2014). Interestingly, membrane attack complex (MAC) is already detectable at the level of the CC and Bruch's membrane (BrM) early in life (Mullins et al., 2014). Second, age-related changes at the level of the BrM may also impair the inter-change between the choroid and outer retina. Senescence of BrM results in a lipid rich interchange barrier (Pauleikhoff et al., 1990), which was later shown to be rich in esterified cholesterol (EC) and linoleate, apolipoprotein (apo) B and E-containing large lipoprotein particles (Curcio, 2018b; L. Wang et al., 2009). This extracellular lipid rich "oil spill" may accumulate as basal linear deposit (BLinD) and eventually form funduscopically visible soft drusen. Most likely, the **impairment of rod-mediated dark adaptation** is attributable to the impaired interchange between the choriocapillaris (CC) and RPE (Lamb and Pugh, 2004; Owsley et al., 2006; Owsley et al., 2007). This functional impairment of the rod visual cycle appears to be followed by a loss of (steady state) dark adapted rod function (Owsley et al., 2000), which is in line with histopathologic findings of a selective vulnerability for parafoveal rod photoreceptors (Curcio and Allen, 1993).

Intermediate AMD with high risk of progression to late AMD is characterized by three distinct, clinically visible lesions, which can be readily summarized as quantitative imaging features (Curcio et al., 2020; M. L. Klein et al., 2008):

- **Soft drusen** constitute the disease defining lesion of AMD. Soft drusen are continuous with basal linear deposit (BLinD) and may be considered as focal accumulation of the same lipid rich material. Soft drusen tend to be spatially concentrated toward the central retina. Therefore, drusen tend to follow the distribution of cone photoreceptors (Curcio, 2018b; Curcio et al., 2020). The underlying mechanism governing BLinD and soft drusen topography is unknown, but may be a result of the delivery of xanthophyll pigments through RPE to Müller cells in the human fovea (Curcio, 2018a).

- **RPD** constitute subretinal deposit (i.e., on the apical side of RPE) and follow approximately the distribution of rod photoreceptors (Steinberg et al., 2013; Zweifel et al., 2010). Moreover, RPD are somewhat disease unspecific and are frequently found in monogenic diseases that impair the interchange across BrM including Pseudoxanthoma elasticum and Sorsby fundus dystrophy (Gliem, Hendig, et al., 2015; Gliem, Müller, et al., 2015). Across diseases, RPD has been identified as a structural biomaker of impaired rod-mediated dark adaptation and steady-state rod sensitivity (Hess et al., 2019; Neely et al., 2017; Pfau et al., 2018).

- **Hyperpigmentation** is the third major risk factor preceding the conversion from intermediate to late AMD. In SD-OCT, hyperpigmentation typically correlates to intraretinal hyperreflective foci, which have been identified in clinicopathologic correlation studies as anteriorly migrated RPE (Curcio et al., 2017; M. L. Klein et al., 2008). The resulting disruption of the RPE is commonly associated with subsequent atrophy formation (Curcio et al., 2017; M. L. Klein et al., 2008). In addition, it was recently shown that hyperreflective foci are associated with delayed rod-mediated dark adaptation (Echols et al., 2020).

Late or advanced AMD is hallmarked by evidence of (former) exudation and/or presence of RPE atrophy as described below in detail.

1.3 Geographic Atrophy

1.3.1 Terminology

Geographic atrophy (GA) may refer to both, the non-exudative late stage of AMD (i.e., diagnosis) as well as the clinical lesion(s) of RPE atrophy. The diagnosis of GA is defined by well-defined, usually more or less circular patches of RPE atrophy, with visibility of the underlying choroidal vessels as well as the absence of neovascularization (Sadda et al., 2018).

1.3.2 Clinical Course

In conjunction with complete atrophy of the overlying outer retina, these foci are thought to constitute absolute scotomata. Initially, patients present often with parafoveal atrophy and preserved BCVA, a phenomenon termed foveal sparing (Sunness et al., 2008). For example, the Age-Related Eye Disease Study 2 (AREDS2) Ancillary SDOCT study demonstrated, that 26.4% develop any GA (central or non-central) over a follow-up of 4 years, while only 15.8% develop central GA (Sleiman et al., 2017). Over time, these foci of atrophy enlarge and coalesce resulting eventually in central atrophy and loss of BCVA (J. P. Sarks et al., 1988).

1.3.3 Histopathology

The histopathology and junctional zone of GA have been described in great detail *in vitro* (Li et al., 2018; J. P. Sarks et al., 1988; S. H. Sarks, 1976; Zanzottera et al., 2016), as well as *in vivo* using SD-OCT (Bearelly et al., 2009; Fleckenstein et al., 2008). The boundary of GA can be defined by the loss of RPE, which may be visualized using funduscopy and fundus autofluorescence (FAF) imaging (Schmitz-Valckenberg, Fleckenstein, et al., 2011). Alternatively, the boundary can be defined by ELM descent, which is nowadays visible in (averaged) SD-OCT B-scans (Li et al., 2018). From the non-atrophic side toward the ELM descent, CC density decreases, while deposits in the sub–RPE-basal lamina space increase and RPE becomes dysmorphic (Biesemeier et al., 2014; Li et al., 2018; Zanzottera et al., 2016). This spatial sequence may be considered as a surrogate of the temporal sequence of degeneration (Zanzottera et al., 2016). Within the atrophic area delimited by the ELM descent, Henle's fiber layer and outer nuclear layer (HFL+ONL) thickness is halved, and comprises predominantly Müller cells (Li et al., 2018). Nevertheless, residual cone photoreceptor nuclei have also been evidenced on the atrophic side of the ELM descent (cf. Figure 2 in Zanzottera et al., 2016) as well as in the context of outer retinal tubulation (Dolz-Marco et al., 2017). The functional implications of these residual cone photoreceptors is unclear (cf. Hypothesis 2 in 1.6 Hypotheses and Specific Aims).

1.3.4 Imaging of Atrophy

Short-wavelength fundus autofluorescence (FAF) confocal scanning laser ophthalmoscopy (cSLO) combined with infrared reflectance (IR) confocal scanning laser ophthalmoscopy (cSLO) imaging were shown to allow for accurate quantification

of lesion size (Lindner et al., 2015; Schmitz-Valckenberg, Brinkmann, et al., 2011; Schmitz-Valckenberg, Fleckenstein, et al., 2011). Foci of GA are characterized by well-defined areas of decreased autofluorescence given the loss of RPE and its inherent fluorophores. More recently, green-emission FAF, which is not absorbed by macular pigment, has been shown to provide even better inter-reader agreement (Pfau et al., 2017).

1.3.5 Prognostic Imaging Biomarkers

A plethora of risk factors have been described for the progression of GA (reviewed in detail in Fleckenstein et al., 2018). The median progression rate of GA was reported to be ∼1.78 mm^2/year (Fleckenstein et al., 2018). Important intraocular prognostic factors for the future progression rate include the baseline lesion size and multifocality as well lesion circularity (faster progression rates in eyes with lower lesion circularity) (Fleckenstein et al., 2018; Sunness et al., 2007). Further, the fundus autofluorescence (FAF) phenotype constitutes an important intraocular prognostic factor, which has been validated in independent cohorts (Fleckenstein et al., 2018; Holz et al., 2007; Schmitz-Valckenberg et al., 2016). In addition, the fellow-eye status represents an established systemic risk factor for GA progression (Fleckenstein et al., 2018). However, correlation (i.e., redundancy) of these prognostic features is evident. It is unclear, how well combinations of these features can predict future progression rates (cf. Hypothesis 4 in 1.6 Hypotheses and Specific Aims).

1.4 Macular Neovascularization

Evidence of ongoing (and former) exudation secondary to MNV in AMD define the exudative late-stage manifestation of AMD (Spaide et al., 2020). MNV may be classified according to its axial location. The spectrum of (MNV) includes type 1 MNV, which manifests in the sub-RPE space, type 2 (MNV) defined by a neovascularization in the subretinal space (i.e., above the RPE) and type 3 MNV (retinal angiomatous proliferation) with new vessels emanating form the retina with possible choroidal anastomoses (Spaide et al., 2020). A further type of MNV termed polypoidal choroidal vasculopathy is common among asian patients and can be considered as a subtype of type 1 MNV (also termed *aneurysmal type 1 MNV*) (Li et al., 2019). All subtypes of MNV can result in devastating loss of visual function if left untreated due to exudation (bleeding and leaking of plasma) (Rosenfeld et al., 2006).

1.4.1 Exudative Activity of Macular Neovascularization

Traditionally, the clinical diagnosis of (MNV) in AMD was equated to exudative late-stage AMD. However, already in 1976 Shirley Sarks reported in one of the hallmark publications of AMD (S. H. Sarks, 1976), that neovascularization is evident in six of 42 eyes (14.3%) and ten of 24 eyes (41.7%) with the clinical diagnoses of intermediate AMD and GA upon *post mortem* histopathologic examination. Today, multimodal imaging allows for *in vivo* diagnosis of treatment-naïve, non-exudative MNV (Carnevali et al., 2016; Querques et al., 2013; Roisman et al., 2016). The key criteria for the identification of non-exudative type 1 MNV are the double-layer

sign (also termed shallow, irregular RPE elevation [SIRE]) in SD-OCT, visibility of a vascular network in OCTA and absence of any signs of exudation in SD-OCT (i.e., absence of intra- and subretinal fluid) as well as in CFP (absence of hemorrhages). Figure 1.1 provides an example of non-exudative type 1 MNV. Based on observational and semi-quantitative data, it has been hypothesized that (non-exudative) type 1 MNV may restore the interchange between the choroid and RPE and thus be protective with regard to RPE atrophy (Capuano et al., 2017; Christenbury et al., 2018). A quantitative proof, especially with regard to treatment-naïve non-exudative type 1 MNV, was previously not available (cf. Hypothesis 5 in 1.6 Hypotheses and Specific Aims).

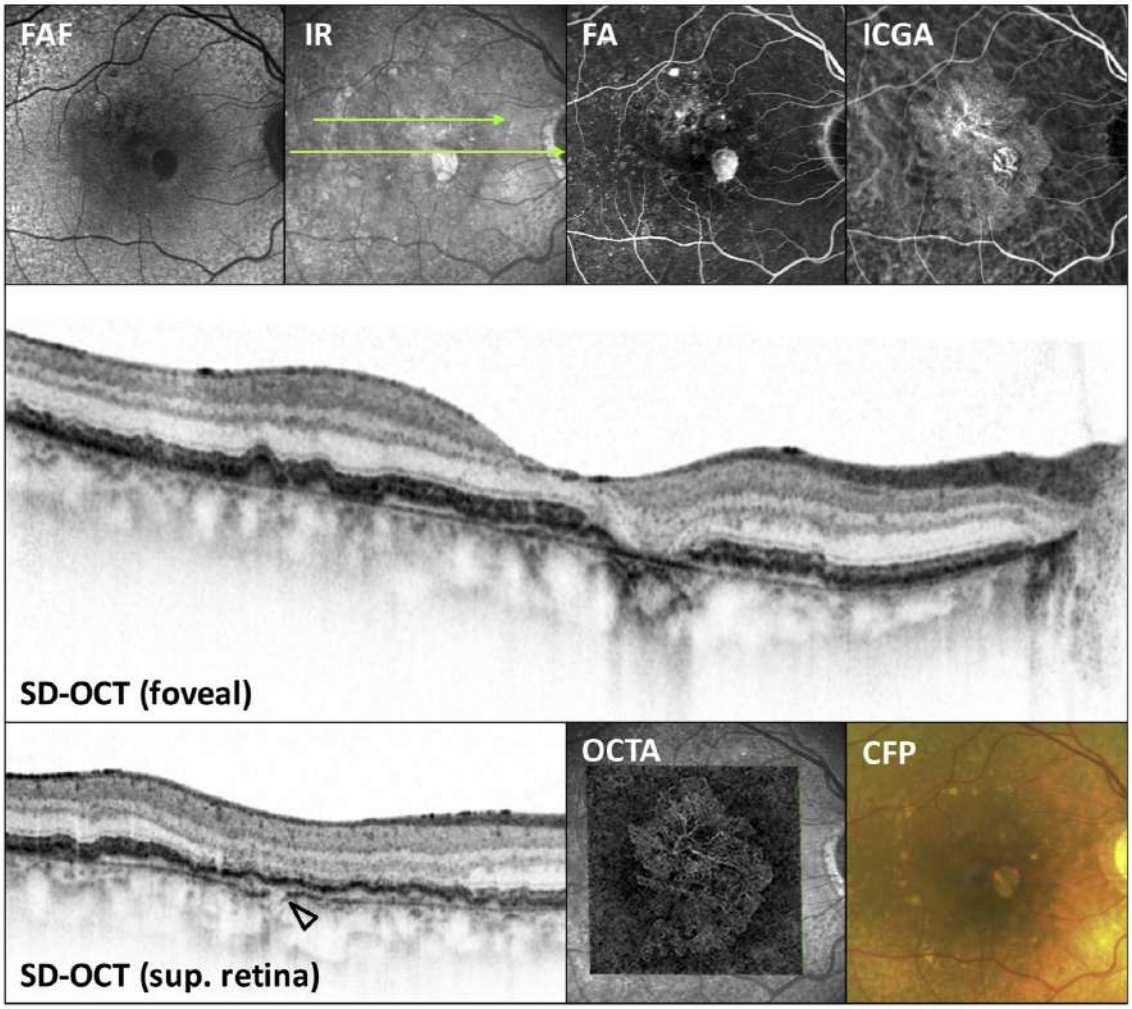

Figure 1.1: The figure shows multimodal imaging data of an eye with non-exudative type 1 MNV. The SD-OCT shows the double-layer sign (also termed shallow, irregular RPE elevation [SIRE]). In addition, the connecting break in BrM can be seen in the extrafoveal B-scan (arrow head).

1.5 Clinical Trial Endpoints in AMD

For MNV involving the fovea, BCVA and SD-OCT-based central retinal thickness (a structural surrogate of BCVA) were successfully applied as clinical trial endpoints

to proof the efficacy of anti-VEGF therapy (Rosenfeld et al., 2006). However, these endpoints are not suitable to quantify the progression of GA, since GA may initially spare the fovea.

In previous trails for therapeutics aimed to slow GA progression, the area of RPE atrophy has served as primary (structural) outcome measure (ClinicalTrials.gov: NCT02247531, NCT02247479, NCT02087085). Fundus-controlled perimetry (FCP), which allows for measurement of retinal sensitivity even in patients with unstable fixation, has been applied as function outcome measure in GA (Heier et al., 2020; Meleth et al., 2011). However, the selected test-pattern (e.g., 10-2 grid) is not congruent with the biological pattern of disease progression. The low spatial resolution of the grid (2° between test points) results in a rather high number of test point (i.e., patient fatigue), while limiting the ability to detect change over time (Pfau, Müller, et al., 2020). A test-pattern tailored specifically to the lesions of a given patient with a high spatial test point density in the junctional zone of GA would be preferable to measure disease progression (cf. Hypothesis 1 in 1.6 Hypotheses and Specific Aims).

By extension, sensitivity estimation based on anatomic imaging (termed *"inferred sensitivity"* here) could provide a workable alternative to quantify sensitivity loss in patients with GA. This strategy has been previously proposed in the context of macular telangiectasia type 2 (Kihara et al., 2019), Leber congenital amaurosis (Sumaroka et al., 2019), and neovascular AMD (von der Emde et al., 2019). A key advantage of this approach would be that structural imaging techniques like FAF, IR, and SD-OCT imaging provide a higher en face resolution compared to FCP testing (5.7 μm/pixel [e.g. Heidelberg Spectralis OCT 2 apparatus] vs. a 128 μm Goldmann III stimulus). Prior to the application of "inferred-sensitivity" as a quasi-functional surrogate outcome, the prediction accuracy and the comparative importance of imaging features have to be analyzed in a disease-specific context (cf. Hypothesis 3 in 1.6 Hypotheses and Specific Aims).

1.6 Hypotheses and Specific Aims

The overarching aim of the five summarized publications (cf. chapter 10) was to identify structural determinants of visual function in the junctional zone of GA and to asses the relevance of these alterations with regard to the future progression of RPE atrophy. Five consecutive hypotheses governed the scope of research and defined the specific aims.

Hypothesis 1: The junctional zone of GA is characterized by a greater degree of rod senstivity loss compared to cone sensitivty loss

> **Background and specific aims:** Multiple lines of evidence point toward a relatively higher vulnerability of rods compared to cones in AMD (cf. Curcio et al., 2000). However, no *in vivo* data existed with regard to the junctional zone of GA. Moreover, previously employed perimetry test-patterns have only a limited ability to detect progression. Accordingly, this project **aimed** to (i) develop a *'patient-tailored'* perimetry workflow to measure function with high spatail-resolution in proximty to GA, (ii) evaluate the relative dysfunction of rod and cone photoreceptors in the junctional zone of GA, and (iii) determine the retest-reliability of measurements in close proximity to the scotomatous lesions as prerequisite for clinical trial protocol development.

Hypothesis 2: Measured sensitivities within the inner junctional zone of GA may not be purely explained by patient-specific false-positive response rates or other reliability indices

> **Background and specific aims:** Both, histopathologic and clinical imaging studies described previously residual (bridging) HFL+ONL within areas of RPE atrophy (cf. Bearelly et al., 2009; Fleckenstein et al., 2008; Li et al., 2018). In the context of ongoing and emerging RPE cell replacement therapies (e.g., NCT02590692), the degree of (any) residual function within RPE atrophy is of relevance as indicator of a 'therapeutic window'. Further, it would define a baseline level of function that a given cell replacement intervention would need to surpass to demonstrate efficacy. Therefore, this study **aimed** to (i) investigate evidence of residual function within areas of RPE atrophy and (ii) determine the possible functional implications of residual HFL+ONL within areas of RPE atrophy.

Hypothesis 3: Outer retinal microstructure correlates closely to retinal function

Background and specific aims: Previous structure-function correlation studies indicate that outer retinal microstructure closely correlates to retinal function (e.g., Steinberg et al., 2016). However, these are mostly based on 'hand-crafted' features (i.e., only few retinal layers thicknesses) and multiple linear regression models to allow for statistical inference. These models tend to perform poorly in the context of multicollinearity (correlation among the input variables). Hence, this project **aimed** to (i) apply a machine learning approach to predict retinal rod and cone photoreceptor sensitivity, and (ii) identify the relative importance the structural determinants for these predictions in a data driven manner.

Hypothesis 4: The FAF phenotype as indicator of wide-spread outer retinal and RPE alterations is prognostic for future RPE atrophy progression independent of lesion shape

Background and specific aims: Variegated risk factors for overall RPE atrophy progression have been described previously. However, it is evident that these factors are not entirely independent factors based on clinical observation (reviewed by Fleckenstein et al., 2018). An example of such *'feature redundancy'* is the *'diffuse trickling'* FAF phenotype, which is characterized by multifocal and multilobular lesions as well as RPD. Accordingly, this study **aimed** to assess the variability in future RPE atrophy progression rates explained by (i) individual and (ii) combinations of previously described risk factors.

Hypothesis 5: Type 1 MNV is associated with a reduced localized progression of retinal pigment epithelium atrophy

Background and specific aims: An impairment of interchange across BrM - due to BrM senescence and/or loss of senescence CC - has been implicated as a precursor of RPE atrophy in AMD. Hypothetically, type 1 MNV, which is located between BrM and RPE, may restore the interchange between the choroid and RPE and thus reduce RPE atrophy progression. Previous clinical observational and semi-quantitative analyses support this hypothesis (Capuano et al., 2017; Christenbury et al., 2018). Hence, this study **aimed** to (i) develop a statistical model to predict *localized* future RPE atrophy progression, and (ii) formally test the hypothesis that type 1 MNV is associated with reduced *localized* and/or *global* RPE atrophy progression.

Chapter 2

Methods

This section represents an overarching summary of the methods of the here presented analyses. The original publications attached as appendices provide a more detailed description of the methods (cf. chapter 10).

2.1 Clinical Studies

The analyses included in this thesis are based on data from four non-interventional clinical studies. Patient data was collected prospectively by the author in the context of the Directional Spread in Geographic Atrophy 2 (DSGA 2, NCT02051998, [ClinicalTrials.gov], PI: M. Fleckenstein) study, as well as an ancillary FCP study. In addition, a normative data study was conducted to obtain normal SD-OCT data and FCP thresholds. These data underlie the analyses presented in result sections 3.1, 3.2, 3.3 and 3.5.

The analyses presented in result section 3.4 are based on a pooled data from the Fundus Autofluorescence imaging in Age-related Macular degeneration (FAM study, NCT00393692) and the original DSGA study (NCT02051998).

Inclusion criteria for patients with GA were presence of unilateral or bilateral GA secondary to AMD defined by: (1) funduscopically well-defined, usually more or less circular patches of RPE atrophy/hypopigmentation, with visibility of the underlying choroidal vessels, (2) presence of AMD defining drusen or hyperpigmentary changes, (3) a FAF phenotype compatible with AMD and (4) a lesion size greater than 0.5 mm^2 (smallest focus) in terms of sharply-demarcated decreased FAF. Exclusion criteria encompassed (amongst other criteria) evidence of (previous) exudative retinal changes (e.g., hemorrhage, exudates, fibrous scar), history of vitro-retinal surgery, retinal co-morbidity or anterior segment diseases impeding retinal imaging. In the context of DSGA and DSGA2, evidence of mimicking monogenic diseases including late-onset stargardt disease and *PRPH2*-associated disease (including central areolar choroidal dystrophy) based on the FAF phenotype constituted an exclusion criterion. Analogously, patients with these diseases were excluded retroactively from the FAM study cohort for the here presented analyses.

Inclusion criteria for patients with normal eyes were the unilateral absence of a anterior or posterior segment disease (with the exception of mild lenticular aging) and/or history of ocular surgery (with the exception of cataract surgery). These subjects were recruited among patients with unilateral eye disease (e.g., rhegmatogenous

retinal detachment) and relatives or companions of patients.

Written informed consent was obtained from every participant following detailed explanation of the research's nature and potential consequences of involvement. All studies adhered to the tenants of the Declaration of Helsinki and were approved by the responsible ethics committee.

Table 2.1 provides an overview of these cohorts with regard to baseline characteristics.

Table 2.1: Patient characteristics

	Normal data	Perimetry study 1a	Perimetry study 1b	Perimetry study 1c	Association of lesion shape and FAF with Atrophy Progression	Association of Type 1 MNV with Atrophy Porgression
Protocol	Normal data study	DSGA2 ancillary study	DSGA2 ancillary study	DSGA2 ancillary study	DSGA and DSGA2	DSGA2
Eyes and patients	40 normal eyes of 40 subjects	25 eyes of 25 patients	36 eyes of 36 patients	41 eyes of 41 patients	296 eyes of 201 patients	118 eyes of 59 patients
Sex	13 female, 27 male	14 female, 11 male	19 female, 17 male	22 female, 19 male	130 female, 71 male	40 female, 19 male
Age in years, mean +/- SD	58.0 +/- 17.4 [range: 21.8 to 82.1]	77.0 +/- 6.8	75.55 +/- 7.93	75.8 +/- 8.4	72.20 +/- 13.08	76.60 +/- 6.65
Best-corrected visual acuity in logMAR, mean +/- SD	n/a	0.53 +/- 0.42	0.51 +/- 0.39	0.51 +/- 0.40	n/a	n/a
Area of RPE atrophy (at baseline) in mm2	n/a	5.20 +/- 4.18 (mean +/- SD)	5.27 +/- 4.44 (mean +/- SD)	6.0 +/- 4.8 (mean +/- SD)	5.2 [2.3; 9.0] (meadian [IQR])	9.15 [7.10 - 11.19] (mean est. [95% CI])

2.2 Clinical Examinations

2.2.1 Clinical Imaging

Patients and control subjects underwent extensive retinal imaging. The imaging protocol (relevant to this thesis) for the DSGA 2 study and the control subjects included: 30° × 30° cSLO FAF and IR imaging centered to the fovea (Spectralis HRA + OCT 2 device, Heidelberg Engineering GmbH, Heidelberg, Germany), 30° × 25° SD-OCT volume with 121 B-scans and averaging (ART) of 25 images (Spectralis HRA + OCT 2 device, Heidelberg Engineering GmbH, Heidelberg, Germany), 3x3 mm and 6x6 mm OCTA imaging centered to the fovea (PLEX Elite 9000, Carl Zeiss Meditec AG, Jena, Germany). The imaging protocol (relevant to this thesis) of the first DSGA study and FAM study included: 30° × 30° cSLO FAF and IR imaging centered to the fovea (Spectralis HRA device, Heidelberg Engineering GmbH, Heidelberg, Germany).

2.2.2 Psychophysical Testing

All patients underwent BCVA testing using ETDRS charts (Ferris and Bailey, 1996).

Fundus-Controlled Perimetry (Publications 1 to 3)

To measure retinal sensitivity and quantify test-retest reliability, patients and control subjects underwent duplicate FCP testing using the S-MAIA device (CenterVue S.p.A., Italy) (reviewed in detail in Pfau, Jolly, et al., 2020). False-positive responses (measured through presentation of supra-threshold stimuli to the optic nerve head [analogous to Heijl-Krakau method in conventional automated perimetry, but with fundus tracking]), the rate of incorrect pressure events out the response window of the S-MAIA apparatus as well as the test duration were considered as "patient-reliability indices" (Olsson et al., 1997). The 95% bivariate shape ellipse area (BCEA) encompassing 95 percent of the fixation points was recorded as measure of fixation stability.

Test-Pattern in Normal Eyes (Publications 1 and 3)

The test-pattern for control subjects consisted of 71 stimuli across the central 18° of the retina. The test points were evenly distributed along five rings at 1°, 3°, 5°, 7°, and 9° (12 stimuli each). In addition, the test-pattern featured test points nasally and temporally at 2°, 4°, 6°, 8° and 10° along the horizontal meridian as well as one central test point.

Patient-Tailored Perimetry (Publications 1 to 3)

For patients with GA, we developed the technique of "patient-tailored perimetry". Following semi-automated annotation of areas RPE atrophy (cf. below) in FAF, an custom software was applied to generate patient-tailored test-patterns. Test points were positioned along iso-hulls (iso-contour lines) surrounding the boundary of GA. The distances of these iso-hulls from the GA boundary were 0.43°, 0.86°,

1.29°, 2.15°, and 3.01°, in addition to one iso-hull within the boundary of GA (-0.645°). The software to create the perimetry patterns was created using MATLAB (MathWorks, USA). The workflow is illustrated in Figure 2.1.

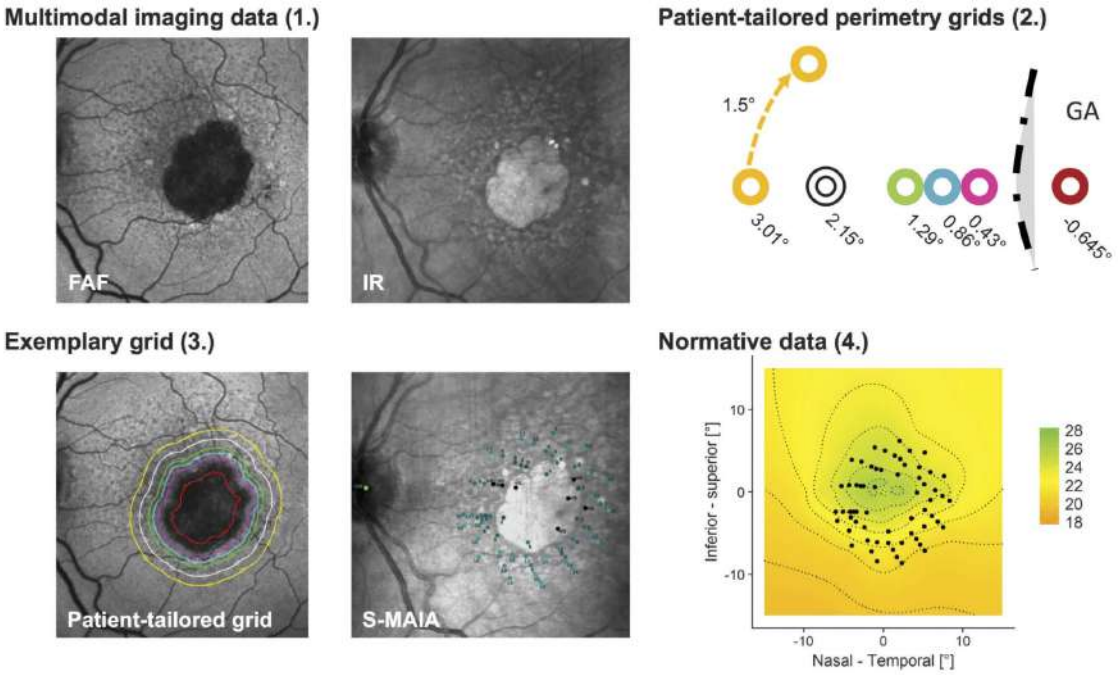

Figure 2.1: Patient-tailored perimetry. Patient-tailored perimetry test-patterns were created based on annotated FAF and IR data. Custom software positioned test points along iso-hulls surrounding the GA boundary. After the perimetry test was performed using the S-MAIA device, the data was registered to a reference coordinate system based on the position of the fovea. Thus, spatially interpolated, age-adjusted, normative data could be extracted for each test point.

Standardization of Perimetry Data (Publications 1 and 3)

Retinal topography has a marked influence on normative mesopic and dark-adapted retinal sensitivity. To standardize perimetry data obtained from patients, normal data from healthy subjects was spatially interpolated in a first step (cf. Supplemental Digital Content 1 in Pfau, Müller, et al., 2020 for details). Subsequently, perimetry data from patients could then be registered to the resulting normative sensitivity maps (Figure 2.1). Sensitivity data from each test point could be standardized in terms of sensitivity loss (i.e., difference of test point specific normal sensitivity and measured sensitivity in a patient).

2.3 Image Analysis Pipeline

En-face Segmentation of GA (Publications 1 to 5)

Combined segmentation of FAF and IR was performed using the RegionFinder software (Heidelberg Engineering GmbH, Heidelberg, Germany) as described previously (Lindner et al., 2015). For publications 1 to 3, a single reader annotated the lesions

given the need to create the patient-tailored perimetry test-pattern during the visit of the patient. For publications 4 and 5, lesions were annotated by a pool of multiple readers. To estimate the inter-rater-variability, 100 eyes of 100 patients were segmented by two readers (cf. publication 4).

SD-OCT Segmentation (Publication 3)

Segmentation of retinal layers was performed with the Heidelberg Eye Explorer (version 1.10.2.0, Heidelberg Engineering, Germany). First, the automated segmentation was applied, followed by two consecutive rounds of manual correction by two different readers. The second reader acted as senior reader. The segmented layers included (i) the inner retina, ranging from the ILM to the OPL/ONL-boundary, (ii) the HFL+ONL, ranging from the OPL/ONL-boundary to the ELM, (iii) IS, ranging from the ELM to the EZ, (iv) OS, ranging from the EZ to the RPEDC, and (v) the RPEDC, which includes RPD, RPE, and sub-RPE-deposits. Similar to previous publications, the hypo-reflective HFL fractions were counted toward the HFL+ONL (Sadigh et al., 2013).

Multimodal Image and Perimetry Data Registration (Publications 2, 3 and 5

For all structure-function analyses (publications 2 and 3) as well as the analysis of the association of type 1 MNV with GA progression (publication 5), multimodal image registration was performed using the Fiji installation of ImageJ (U. S. National Institutes of Health, Bethesda, MD, USA). Vascular bifurcations served as landmarks for the registration. Images were then aligned using an affine transformation as implemented in the *Landmark Correspondence* function of Fiji. For the structure-function analyses (publication 2 and 3), FCP data were registered to the SD-OCT volume. For the analysis of GA progression in dependence of the presence of type 1 MNV (publication 5), GA progression was first quantified using the RegionFinder software in FAF images. The RegionFinder software registers automatically the complete longitudinal FAF image sequence of a given eye. Then, the labeled OCTA data (maps annotated for the presence of type 1 MNV) were registered to the annotated FAF image sequence using Fiji (cf. Figure 2.4).

Extraction of Point-wise Retinal Reflectivity and Thickness Values (Publication 3)

Following the multimodal data registration, the SD-OCT thickness and reflectivity values could be extracted for each test point for all segmented retinal layers. For each layer, three types of reflectivity maps were available: a minimum-, mean-, and maximum-intensity projection. The region-of-interest function in Fiji was applied to extract the respective imaging biomarkers at the exact location and with the specific diameter (Goldmann III, 0.43° diameter) of each stimulus (Figure 2.2).

Extraction of Shape-Descriptive Factors (Publication 4)

Shape-descriptive factors were extracted with an ad-hoc developed Fiji plug-in (Figure 2.3). This tool converted lesion annotations from the RegionFinder software

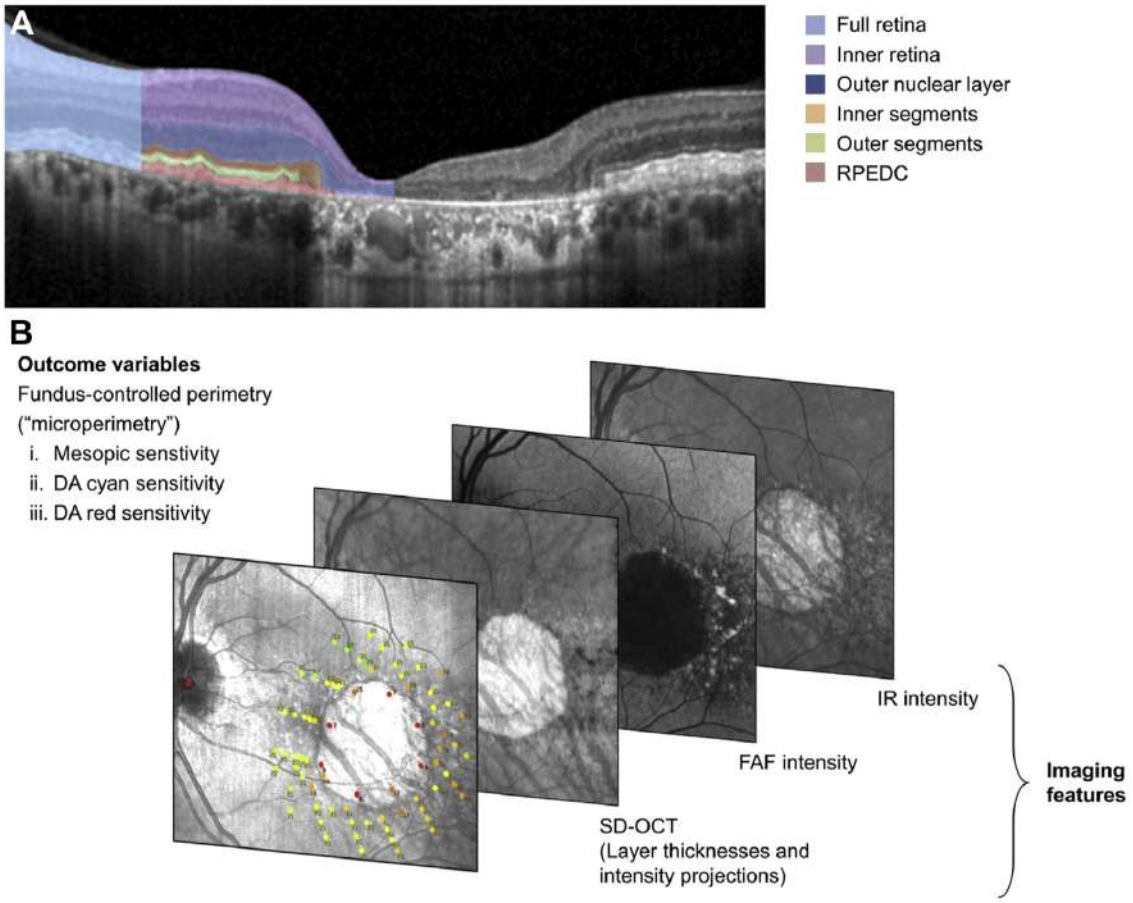

Figure 2.2: Multimodal image and perimetry data registration. The SD-OCT B-scan shows an exemplary segmentation. Based on vascular bifurcations, data from SD-OCT, IR, FCP, (as well as OCTA, cf. publication 5) could be aligned in a precise manner. For structure-function correlation, imaging features were extracted for region-of-interests corresponding to the location and area of each Goldmann III stimulus.

into binary masks. These could then be used to extract the area of RPE atrophy, maximum caliper diameter of the lesion ($\text{Feret}_{\text{max}}$), minimum caliper diameter of the lesion ($\text{Feret}_{\text{min}}$). In addition, the tool was used to extract the lesion perimeter (cumulative circumference of the lesion) as well as the lesion circularity ($(4 \times \pi \times Area)/Perimeter^2$). The circularity is a measure of how closely the shape of an object approaches that of a mathematically perfect circle (value range from 0 to 1).

Classification of macular neovascularization (Publication 5)

For the analysis of the association of MNV with RPE atrophy progression, MNV lesions were sub-classified according to the presence/absence of MNV and the exudative activity of the MNV lesions. Specifically, the subgroups included:

- Eyes with RPE atrophy, but no evidence of MNV (synonymous to the diagnosis GA)
- Eyes with RPE atrophy and treatment-naïve quiescent MNV (i.e., no evidence

or clinical record of prior exudation, cf. Figure 1.1)

- Eyes with RPE atrophy and (former) exudative MNV

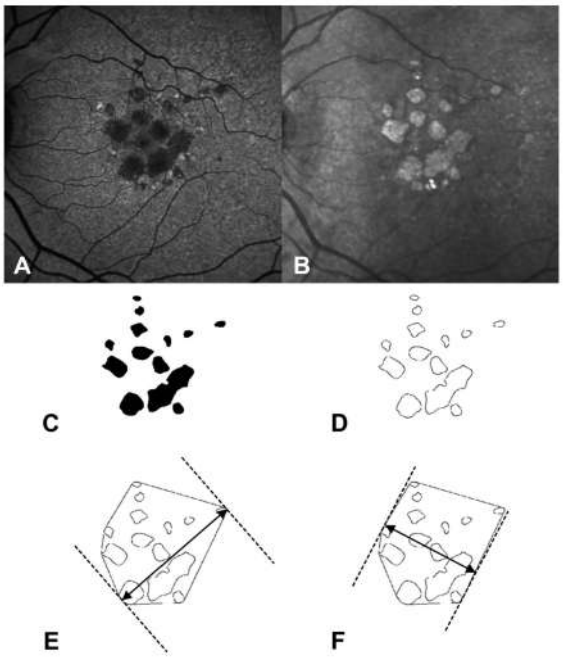

Figure 2.3: Extraction of shape-descriptive factors. The custom plug-in for ImageJ converted the lesion annotations (C) to outlines (D). Subsequently, shape-descriptive factors such as the maximum and minimum caliper (Feret) diameter of the lesion (E and F) could be extracted in an automatic manner.

2.4 Statistical Analyses

All statistical analyses were performed using the software environment R (R Development Core Team 3.0.1., 2013). Normally distributed variables were summarized by their mean and standard deviation. Non-normally distributed variables were summarized by their median and interquartile range. Linear mixed model analyses were performed using the R library lme4 (Bates et al., 2015). Visual acuity was converted to the logarithm of the Minimum Angle of Resolution (logMAR).

2.4.1 Analysis of Retinal Sensitivity in the Junctional Zone (Publication 1)

First, the point-wise retest-reliability was analyzed. For all three types of testing, the coefficient of repeatability was computed. The coefficients of repeatability indicates the value, below which the absolute difference of two measurements would be with 95% probability (Bland and Altman, 1999). In addition Bland-Altman plot were used to examine the association of the underlying sensitivity with the variability. Linear mixed models with test points nested in eye as random effects term were used to examine, whether the distance to the GA boundary or the underlying sensitivity

(both included as independent variables) are associated with the point-wise retest-variance (dependent variable). Second, the association of the actual sensitivity loss (dependent variable) in dependence of the distance to the GA boundary (independent variable) was analyzed using linear mixed models (with test points nested in eye as random effects term) for all three types of testing. Last, we determined the percentage of test points that were rod-mediated (both, the cyan and red stimulus), mixed-mediated (cyan stimulus rod-mediated, red stimulus cone-mediated) or indeterminate based on the spectral sensitivity difference (cf. S. Jacobson et al., 1991 for details).

2.4.2 Analysis of Sensitivity within Atrophy (Publication 2)

Sensitivity measurements from within GA (i.e., at the -0.645° iso-hull) are characterized by a highly skewed skewed (non-normal) distribution. Thus, to quantify the retest reliability, we summarized the percentages of the absolute test-retest difference categories (0 dB, <2 dB, <4 dB, and <6 dB).

Based on the patient-specific rate of false-positive responses, and the test point-specific initial test brightness and the staircase strategy, we developed a model to predict the expected sensitivity measurements for the assumption of an absolute scotoma (i.e., trigger pressure events are fully attributable to false-positive responses). For each test point, the expected value was obtained by running this simulated staircase procedure 10.000.

Linear mixed models (with test points nested in eye as random effects term) were applied to examine, whether the discrepancy between measured and expected sensitivities (dependent variable) differed significantly from 0. Moreover, we examined using linear mixed models, whether this sensitivity discrepancy (dependent variable) is associated with (1.) indicators of inaccurate responses or fatigue (age, examination duration, false-positive response rate for catch trials [Heijl-Krakau method], wrong pressure event rate, initial testing brightness), (2.) indicators of inaccurate stimulus projection due to insufficient fundus tracking (bivariate contour ellipse area), or (3.) indicators of genuine retinal sensitivity (outermost visible retinal layer).

2.4.3 Machine-Learning to Predict Retinal Sensitivity (Publication 3)

Prior to the predictive modeling, the SD-OCT features (thickness and reflectivity values) were converted to Z-scores using normative data. This standardization was implemented to adjust for topographic variation of layer thickness and reflectivity values. Retinal sensitivity values of patients were converted to sensitivity loss based on the difference to topographically corresponding normative data.

Since the putative predictors of retinal sensitivity (SD-OCT layer thickness and reflectivity values) were highly correlated, we applied random forest regression as predictive model. For the first scenario (S1, "prediction of sensitivity without patient-specific training data"), nested re-sampling was applied to estimate the model accuracy (outer patient-wise leave-one-out cross-validation), while simultaneously tuning the random forest parameter mtry (nested inner 5-fold cross-validation with patient-wise splits). For the second scenario (S2, "prediction of sensitivity

with limited patient-specific sensitivity data"), half of the patient-specific test results (i.e., data from every other test point along each iso-hull) were added to the training information, and only the other half of the patient-specific data served as evaluation data to obtain an estimate of the model accuracy. In addition, the eye ID was added in scenario 2 through one-hot encoding as predictor to the model.

For both scenarios, three predictive feature sets (A, B, respectively. C) were assessed:

- S1A [i.e., Scenario 1 with feature set A] and S2A: imaging features only (26 candidate variables)
- S1B and S2B: imaging features and "patient reliability indices" (30 candidate variables)
- S1C and S2C: imaging features and "patient reliability indices" and fixation stability (31 candidate variables)

Null models were computed for both, S1 (prediction for each patient simply based on the average sensitivity loss of the other patients) and S2 (prediction based on the patient-specific average sensitivity loss from every other test point along each iso-hull). The mean absolute error (MAE) between predicted and observed sensitivity loss served as measure of model performance. Linear mixed effects models considering the MAE as dependent variable and patient as random effect term were used to examine, whether the feature set is associated with the model performance. The permutation importance (increase in mean squared error [% Inc MSE]) was evaluated to understand the contribution of the predictors.

2.4.4 Modeling of Overall Atrophy Progression (Publication 4)

Two scenarios were evaluated for the prediction of overall GA progression rates: Scenario 1 ("prediction with no patient-specific prior data") based on patient-wise leave-one-out cross-validation, and scenario 2 ("prediction with prior observation of the patient") based on visit-wise leave-one-out cross-validation. Linear mixed models were applied to predict the square-root progression rate of GA (mm/y).

As candidate feature sets, we considered all shape descriptive factors individually, a "clinical trial inclusion model" based on previous publications (included the prior square-root GA area, FAF phenotype, and focality), and a full model with all shape-descriptive factors. The coefficient of determination (R^2) served as measure of model performance.

2.4.5 Modeling of Localized Atrophy Progression (Publication 5)

The localized progression of RPE atrophy in topographic relation to the MNV lesion was analyzed using mixed effects logistic regression with pixel nested in eye nested in patient as random effects term. The pixel/point-specific binary outcome of the next visit (atrophic or non-atrophic) was the dependent variable. Independent variables included pixel/point-specific factors such as the distance to the RPE atrophy

boundary, the distance to the fovea, localized presence of MNV, horizontal position, and vertical position. In addition, the follow-up time and overall diagnosis of the eye (RPE atrophy without MNV, RPE atrophy and treatment-naïve quiescent MNV, or RPE atrophy and exudative MNV) were included as predictors (Figure 2.4). The spatial overlap (Dice coefficient) between 5-fold cross-validated predicted and observed RPE atrophy progression was evaluated to estimate the model performance. The statistical effect size of the localized presence/absence of MNV for the prediction of the localized future progression of RPE atrophy was the primary outcome.

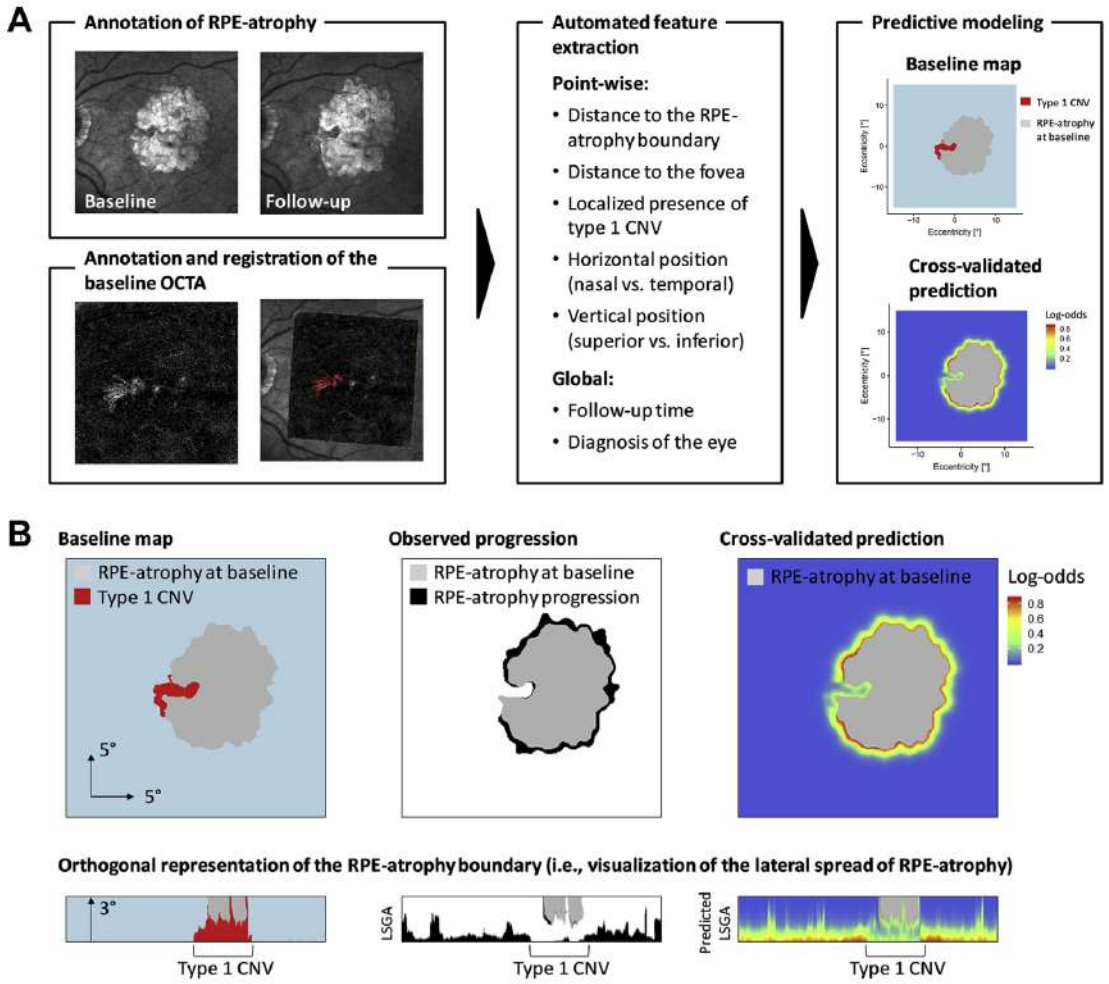

Figure 2.4: Feature extraction and modeling to predict localized atrophy progression. The figures shows how predictive features were extracted from the imaging data of the patients and applied in a mixed effects logistic regression model to predict localized atrophy progression. This allowed to formally test the hypothesis, that treatment-naïve quiescent MNV slows the progression of RPE atrophy.

Chapter 3

Results

3.1 Development of Patient-Tailored Perimetry for Geographic Atrophy[1]

3.1.1 Cohort Description

A total of 25 patients with GA secondary to AMD (age [mean ± SD] 77.0 ± 6.8 years [range 64.1 to 89.7 years]) with a mean visual acuity of 0.53 ± 0.42 logMAR (20/68 Snellen equivalent) were included in this analysis. Forty healthy eyes of 40 subjects served as normal data.

3.1.2 Point-wise Retest-Reliability

The point-wise coefficients of repeatability were ±6.64 dB for mesopic, ±5.78 dB for DA cyan, and ±7.24 dB for DA red testing.

Regarding factors influencing retest-reliability, higher retinal sensitivity was associated with minimally less retest variance for mesopic testing ([slope estimate ± SE] -0.26 ± 0.08 db^2/dB; $P < 0.01$). The iso-hull (i.e., distance to the GA boundary) had no influence on the retest variance ($P = 0.26$). Similarly, in DA cyan testing, the retinal sensitivity was associated with the retest variance (+0.28 ± 0.07 db^2/dB; $P < 0.001$), but no association was evident between the iso-hull and retest-variance ($P = 0.45$). For DA red testing, both the test sensitivity ($P = 0.017$) and distance to the GA boundary ($P < 0.001$) were associated with the retest variance. A likelihood ratio test for DA red testing revealed that the model including only the distance to GA boundary as fixed effect was superior to a model including both variables as fixed effect. In summary, differences in retest variance across all three types of testing and all iso-hulls were rather minor (Figure 3.1).

[1]This section constitutes a synopsis of the results of *Pfau et al. Mesopic and DA Two-Color Fundus-controlled Perimetry in Geographic Atrophy Secondary to Age-Related Macular Degeneration. Retina. 2020 Jan;40(1):169-180.* The original publication is attached as appendix (page 76*ff*).

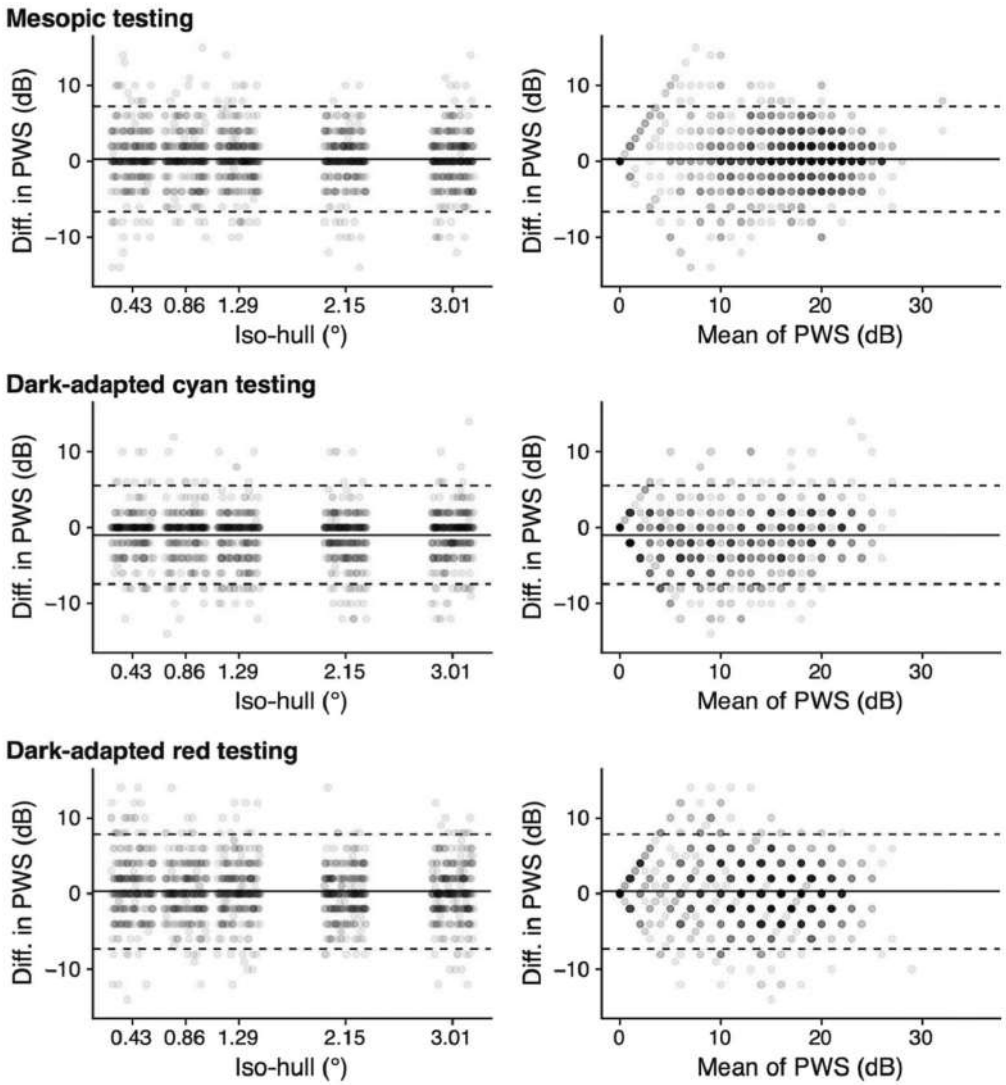

Figure 3.1: Point-wise retest-reliability. The left column shows the point-wise sensitivity (PWS) test-retest difference in dependence of the distance to the GA boundary. The right column shows the PWS test-retest difference in dependence of the underlying sensitivity (i.e., Bland-Altman plots). The retest-reliability was similar across a wide range of sensitivity values. The solid line denotes the mean difference, dashed lines denote the 95% limits of agreement.

3.1.3 Retinal Function in the Junctional Zone of Geographic Atrophy

Sensitivity measurements from within GA (i.e., at the -0.645° iso-hull) were excluded from the subsequent analysis due to the highly skewed skewed (non-normal) distribution of the results. The median (IQR) sensitivity loss for these test points was 22.9 dB [23.4 to 19.5 dB] for mesopic, 18.5 dB [19.7 to 17.0 dB] for DA cyan testing, and 20.8 [21.8 to 17.4 dB] for DA red testing.

For test points outside of GA, the distance to GA exhibited a marked association with the mesopic sensitivity loss ($P < 0.001$). According to a post hoc test, sensitivity varied significantly between 0.43° (sensitivity loss of [mean ± SE] 10.68

± 1.05 dB) and 0.86° (8.97 ± 1.05 dB) as well as between 0.86° and 1.29° (-7.83 ± 1.05 dB). No distinct differences ($P > 0.05$) between the mesopic sensitivity loss at 1.29°, 2.15° (7.42 ± 1.04 dB) and 3.01° (7.27 ± 1.04 dB) was evident.

For DA cyan testing, the distance to GA had an influence on the sensitivity as well. Post hoc comparison revealed marked differences ($P < 0.01$) in sensitivity loss between 0.43° (16.25 ± 1.37 dB) and 0.86° (14.95 ± 1.37 dB) as well as a significant difference ($P < 0.01$) between 1.29° (14.08 ± 1.36 dB) and 2.15° (12.69 ± 1.36 dB).

For DA red testing, distance to GA had a similar relationship with sensitivity as for mesopic testing. The sensitivity loss varied distinctly ($P < 0.001$) between 0.43° (12.57 ± 1.31 dB) and 0.86° (11.06 ± 1.31 dB), between ($P < 0.01$) 0.86° and 1.29° (10.05 ± 1.31 dB) and between ($P < 0.05$) 1.29° and 2.15° (9.28 ± 1.31 dB). The sensitivity loss did not differ significantly between 2.15° and 3.01° (9.10 ± 1.31 dB).

In summary, a distinct increase in mesopic and DA red sensitivity, which levels off for test points more distant than 1.29° or 2.15° to the GA boundary, was evident as well as more pronounced overall DA cyan sensitivity loss.

3.1.4 Rod versus Cone Degeneration

Comparison of the point-wise DA cyan-red sensitivity differences revealed that the fraction of test points, where both stimuli are rod-mediated increased with increasing distance to the GA boundary.

Interestingly, point-wise comparison of DA red and mesopic sensitivity losses revealed a strong linear correlation between mesopic and DA red sensitivity loss. This relationship could be described by a simple linear mixed model with an intercept close to zero (0.58 dB) and a slope of 0.89 dB/dB ($R^2 = 0.77$). In contrast, the relationship between mesopic and DA cyan sensitivity loss was nonlinear. DA cyan sensitivity loss was evident in numerous test points with quasi-normal mesopic sensitivity. In contrast, all test points with mesopic sensitivity loss exhibited DA cyan sensitivity loss (Figure 3.2).

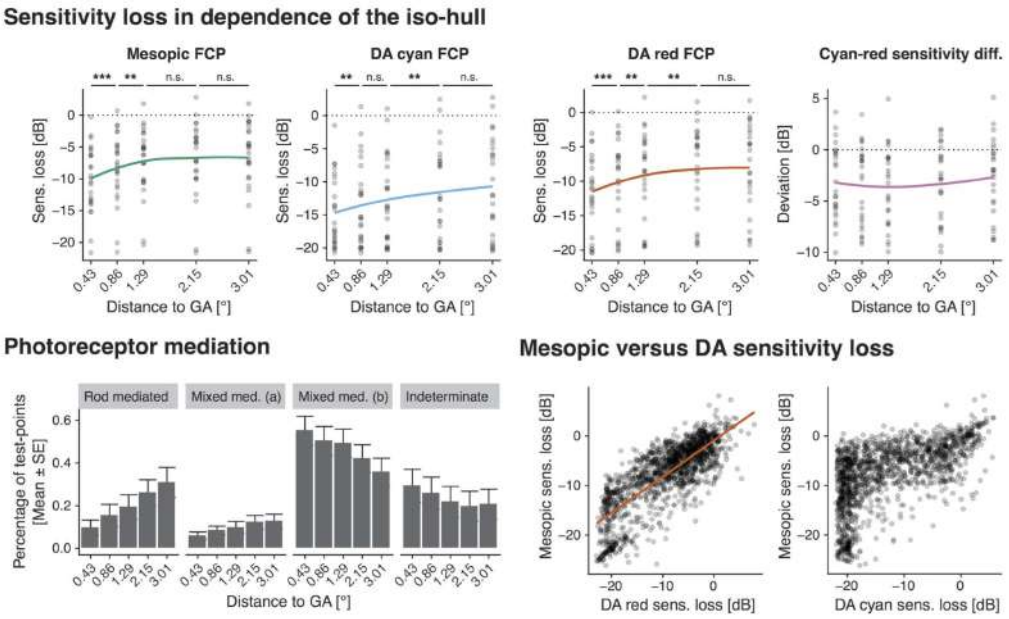

Figure 3.2: Retinal sensitivity in the junctional zone of GA. The upper row shows the change in retinal sensitivity loss with increasing distance to the GA boundary. The lower left panel shows the proportion of stimuli with rod mediation (both, cyan and red stimulus), mixed mediation (cyan stimulus mediated by rod photoreceptors, red stimulus mediated by cone photoreceptors [a and b denote, whether the red threshold is within normal limits]) and indeterminate mediation. The lower right panel shows the point-wise relationship between mesopic sensitivity loss and DA red and DA cyan sensitivity loss, respectively.

3.2 Residual Function within Areas of Geographic Atrophy[2]

3.2.1 Cohort Description

A total of 36 eyes of 36 patients with GA secondary to AMD (age [mean ± SD] 75.6 ± 7.9 years [range, 58.1–89.7 years]) with a mean visual acuity of 0.51 ± 0.39 logMAR (approximately 20/40 Snellen equivalent) were available for the analysis. On average, 6.4 ± 2.7 test points per eye were confined to the -0.645° iso-hull and thus included. For all of these test points, duplicate mesopic, DA cyan, and red testing sensitivity measurements were available (i.e., total of 1380 threshold measurements within atrophy [approx. 3 types of testing × average of 6.4 test points × 2 replications × 36 patients]).

The retest-reliability was moderate for these selected test points. Specifically, identical values for the test and retest were obtained for (median, interquartile range [IQR]) 42.9% (24.3% – 67.5%) of all test points in mesopic testing, for 69% (46.9% – 100%) and 57.1% (33.3% – 67.9%) of all test points in DA cyan and DA red testing, respectively.

[2]This section constitutes a synopsis of the results of *Pfau et al. Light Sensitivity Within Areas of Geographic Atrophy Secondary to Age-Related Macular Degeneration. Invest Ophthalmol Vis Sci. 2019 Sep 3;60(12):3992-4001.* The original publication is attached as appendix (page 88*ff*).

3.2.2 Configuration of the Inner Junctional Zone

Three major subtypes of the inner junctional zone configuration were observed at the site of functional testing (i.e., -0.645° iso-hull, Figure 3.3): (1) cRORA at GA boundaries with a close proximity of the ELM descent and OPL/INL descent (n = 135 of test points); (2) residual HFL+ONL within areas of RPE atrophy with (partial) bridging of the area of RPE atrophy (n = 83); and (3) ORTs (n = 12). The inter-rater reliability for the classification was substantial (unweighted Cohen's κ for two raters = 0.77).

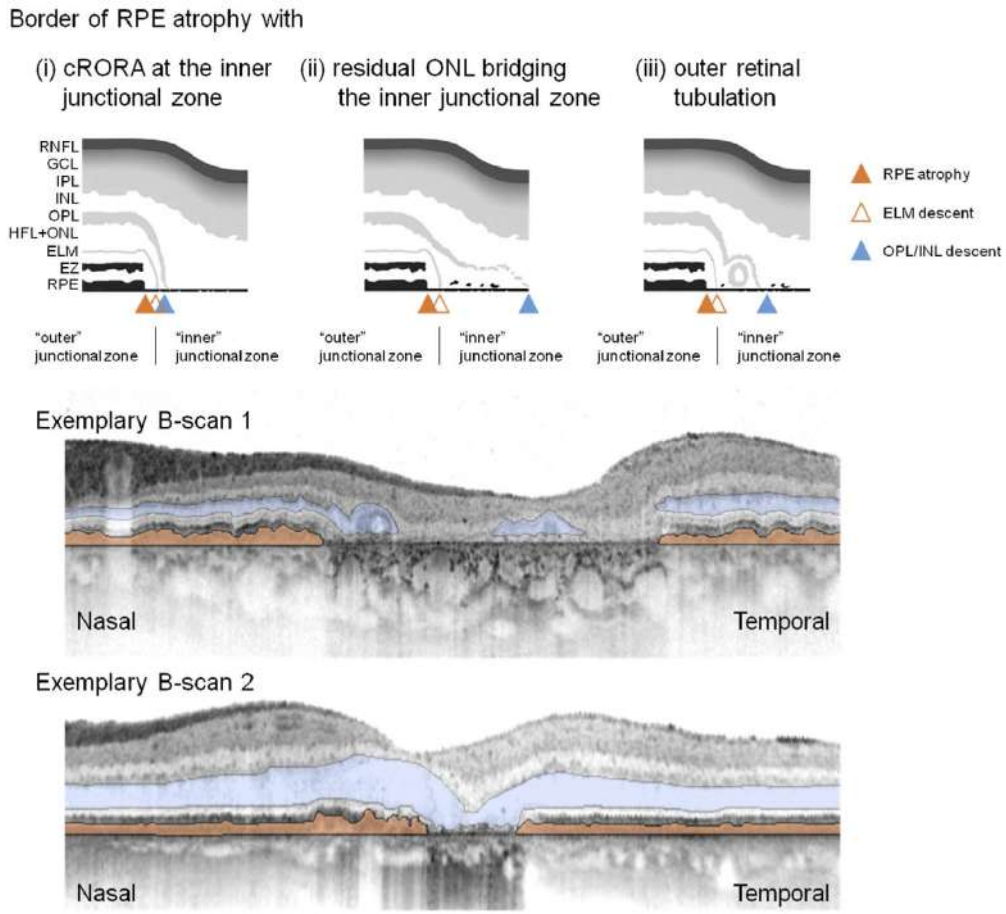

Figure 3.3: Classification of the inner junctional zone. The upper row shows the three identified subtypes of the inner junctional zone. The exemplary B-scan 1 shows on the nasal side an ORT, and cRORA at the temporal boundary. The exemplary B-scan 2 is an example of residual HFL+ONL within RPE-atrophy.

3.2.3 Expected Sensitivity Based on False-Positive Responses versus Measured Sensitivity

Based on the patient-specific false-positive response rate, the staircase strategy (4-2), and the initial testing brightness of the staircase for each test point, the expected values under the assumption of an absolute scotoma could be simulated for each test point. Mixed model analysis confirmed that the measured values were significantly higher as compared to the expected values for absolute scotomata (Figure 3.4). The

discrepancy between measured and expected values was (mean ± standard error) +6.92 ± 0.86 dB for mesopic, +2.57 ± 0.56 dB for DA cyan, and +4.93 ± 0.74 dB for DA red testing. Furthermore, the percentage of unlikely measurements (i.e., point-wise measurements with a probability of $P < 0.05$ for the assumption of absolute scotoma) was (median [IQR]) 34.8% (14.3% – 62.8%) for the first mesopic examination, and 35.4% (25% – 54.8%) for the second mesopic examination and therefore markedly higher than 5%. For DA cyan testing, the median percentage of unlikely measurements was lower, with 4.5% (0% – 37.5%) for the first examination and 0% (0% – 27.6%) for the second examination. For DA red testing, the median percentage of unlikely measurements was 31% (14.3% – 64.4%) for the first examination, 25% (0% – 50%) for the second examination.

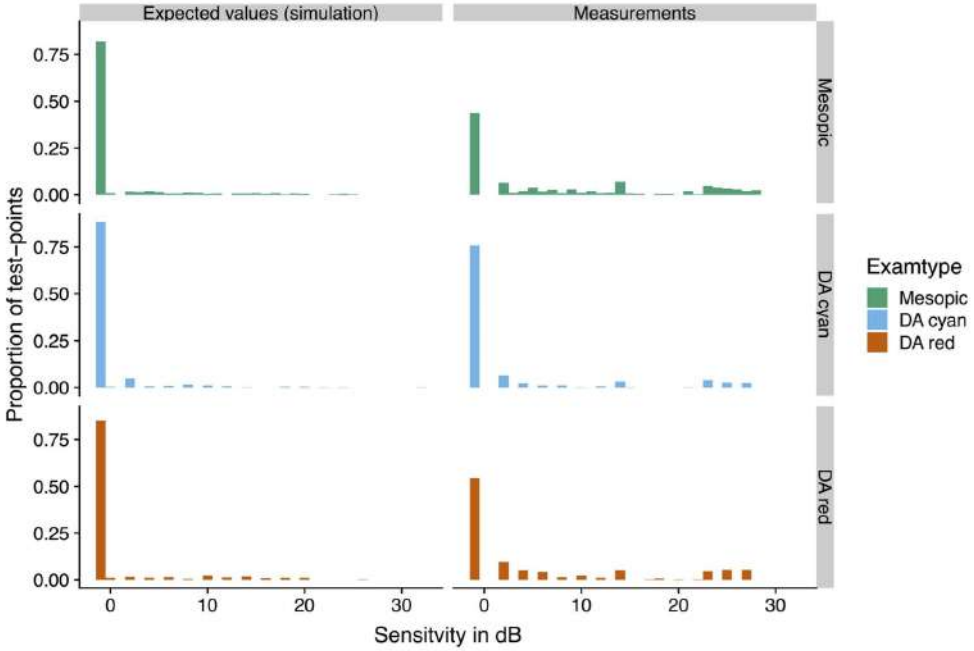

Figure 3.4: The figure shows for all three types of testing (rows) the expected results (simulation with the assumption of an absolute scotoma and with consideration of the patient-specific false-positive response rate, the staircase strategy, and the initial testing brightness) against the measured values (right column). A discrepancy between expected and measured sensitivity is evident.

3.2.4 Structure-Function Correlation and Patient Reliability Indices

For mesopic testing, the outermost layer in SD-OCT exhibited as a fixed effect a significant association with this discrepancy (likelihood ratio test, $P < 0.001$) as well as the false-positive response rate ($P < 0.001$). A post hoc test revealed that the mean discrepancy in measured versus expected sensitivities was significantly higher for test points with residual HFL+ONL versus OPL/INL as the outermost layer in SD-OCT (+5.96 ± 0.98 dB, $P < 0.001$), while the sensitivity discrepancy between test points at ORTs versus OPL/INL differed not significantly (+2.65 ± 2.13 dB, $P = 0.25$).

For DA red testing, the results were similar. The outermost layer in SD-OCT (likelihood ratio test, $P < 0.001$) and the initial testing brightness ($P = 0.0126$), as well as the false-positive response rate ($P < 0.001$), exhibited as fixed effects a significant association with the discrepancy in measured versus expected sensitivity. The post hoc test revealed, that this discrepancy differed significantly between test points with HFL+ONL versus OPL/INL as the outermost layer in SD-OCT (+5.19 ± 0.90 dB, $P < 0.001$), while no difference was observed for test points at ORTs versus OPL/INL (+3.32 ± 1.96 dB, $P = 0.180$). Test points with HFL+ONL as outermost layer exhibited a significantly reduced point-wise DA cyan-red sensitivity difference (-5.01 ± 1.07 dB, $P < 0.001$).

For DA cyan testing, neither the outermost layer in SD-OCT nor any other of the probed variables exhibited as a fixed effect a significant association with the discrepancy in measured versus expected sensitivity as indicated by a likelihood ratio test.

Two exemplary patients with the schematic staircase results and the corresponding SD-OCT images are provided for clarification of the results (Figure 3.5).

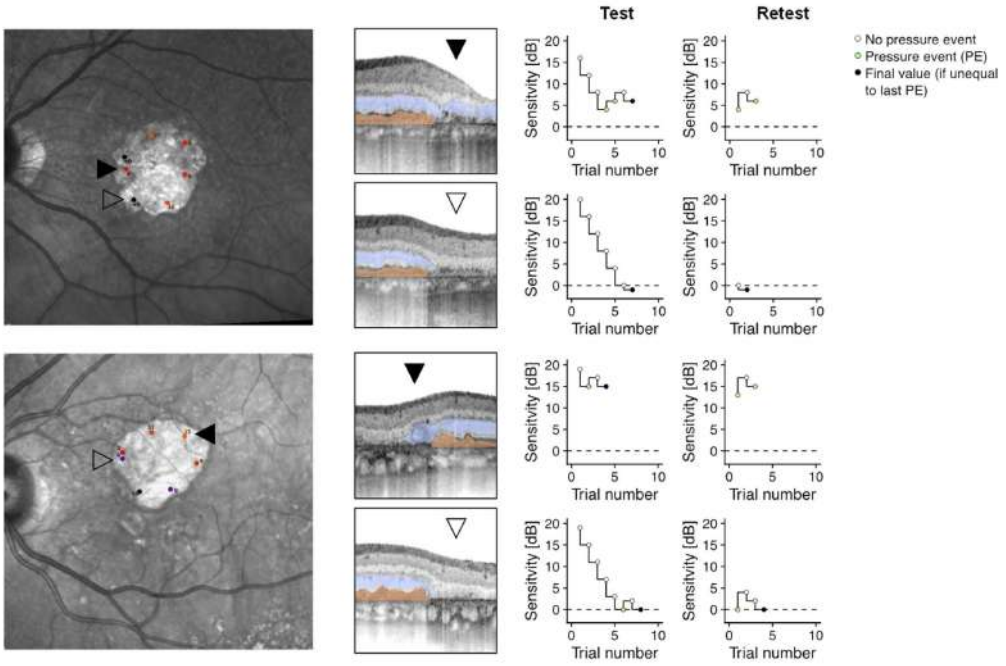

Figure 3.5: In both of these two exemplary patients, test points visible to the patient (*opaque arrowhead*) and invisible to the patient (*transparent arrowhead*) were evident as highlighted by the results of the first and second perimetry tests (staircase diagrams). The upper patient exhibited at the location of the *opaque arrowhead residual* HFL+ONL within GA, the lower patient had at the location of the *opaque arrowhead* an ORT.

3.3 Structural Determinants of Retinal Sensitivity[3]

3.3.1 Cohort Description

A total of 41 eyes of 41 patients with GA secondary to AMD (age [mean ± SD] 75.8 ± 8.4 years) with a mean visual acuity of 0.51 ± 0.40 logMAR were availabe for the analysis.

3.3.2 Prediction Accuracy for an 'Unknown Patient' (scenario 1)

Patient-wise leave-one-out cross-validation (LOO-CV) was implemented to estimate the prediction accuracies of "inferred sensitivity" for an unknown patient (scenario 1). For mesopic sensitivity, the prediction accuracy based on imaging information only (feature set S1A) was (MAE [95% CI]) 4.64 dB [4.02, 5.25]. Neither addition of "patient reliability indices" (feature set S1B) nor of fixation stability (feature set S1C) led to an improved prediction accuracy. For DA cyan testing (4.89 dB [4.29, 5.49]) and for DA red analyzing (4.4 dB [3.89, 4.91]), the predictions accuracies were similar based on the imaging features only (S1A). Again, neither inclusion of "patient reliability indices" (S1B) nor of fixation stability (S1C) enhanced the prediction accuracy (cf. Table 2 in publication 3 [page 98*ff*]).

3.3.3 Prediction Accuracy for 'Patients with Prior Perimetry Data' (scenario 2)

Since some patient characteristics may not be adequately be reflected by SD-OCT data (e.g., lens opacification), we investigated whether addition of patient specific perimetry data enhances the prediction accuracy for the remaining test points. For mesopic testing, the prediction accuracy was better for scenario 2 (S2A, 3.14 dB [2.9, 3.39]), and varied significantly in dependence of the feature set (likelihood ratio test, $P < 0.001$).

Similarly, for both types of DA testing, the prediction accuracy improved significantly ($P < 0.001$) with inclusion of "patient reliability indices" (DA cyan testing: 2.92 dB [2.6, 3.25]; DA red testing: 2.86 dB [2.58, 3.14]), and even further with addition of the fixation stability to the feature set (DA cyan testing: 2.86 dB [2.54, 3.19]; DA red testing: 2.77 dB [2.5, 3.04]).

The prediction accuracy was similar across variable degrees of sensitivity loss, with slightly higher prediction errors for test points with sensitivity loss in the range of 15 dB (Figure 3.6). For severe sensitivity losses of approx. 20 dB, sensitivity losses (both, predicted and measured) were truncated by the floor of this dynamic range of the S-MAIA device (Figure 3.6).

[3]This section constitutes a synopsis of the results of *Pfau et al. Determinants of Cone- And Rod-Function in Geographic Atrophy: AI-based Structure-Function Correlation. Am J Ophthalmol. 2020 Apr 11;S0002-9394(20)30170-7.* The original publication is attached as appendix (page 98*ff*).

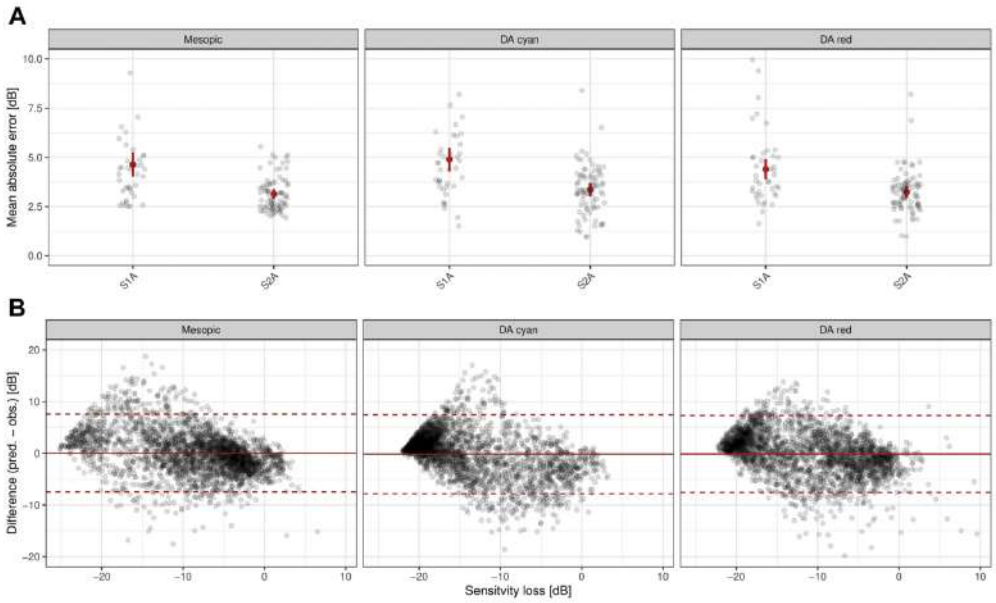

Figure 3.6: The upper row shows the patient-wise estimates for the prediction accuracy in dependence of the type of testing (panels) and in dependence of the scenario (S1A - prediction based on imaging data; S2A - prediction based on imaging data with addition with patient specific information [i.e., addition of every second test point]). The lower rows shows the Bland-Altman plots for S2A (red solid line denotes the mean difference, red dashed lines denote the 95% limits of agreement).

3.3.4 Feature Importance

For the prediction of mesopic sensitivity, the feature importance of the HFL+ONL thickness (35% IncMSE) was markedly higher as compared to the importance of all other predictors. The complete retinal thickness (27.2% IncMSE), as well as the inner retinal thickness (20.4% IncMSE) comprised the third and second most important features. For prediction of DA cyan sensitivity, the HFL+ONL thickness (42.2% IncMSE) also represented the most important feature, followed by the complete retinal thickness (23% IncMSE), and the RPEDC thickness (21.1% IncMSE). For DA red sensitivity, the HFL+ONL thickness (53.7% IncMSE) comprised again the most important feature, followed by the full retinal thickness (33.4% IncMSE), and RPEDC thickness (21.8% IncMSE). HFL+ONL thickness was across all three kinds of testing an outlier in terms of feature importance (Figure 3.7). Moreover, features related to SD-OCT layer thicknesses seemed to exhibit generally a higher feature importance compared with features related to signal intensity.

3.3.5 Structure-Function Correlation and Cone versus Rod Dysfunction

Plotting of the feature contribution of the HFL+ONL thickness (i.e., the contribution of HFL+ONL thickness toward retinal sensitivity after accounting for the contribution of the other predictors) demonstrated, that HFL+ONL thinning was associated with a marked sensitivity loss for all three types of testing (Figure 3.8). However, the amount of sensitivity loss per Z-score of HFL+ONL thinning varied

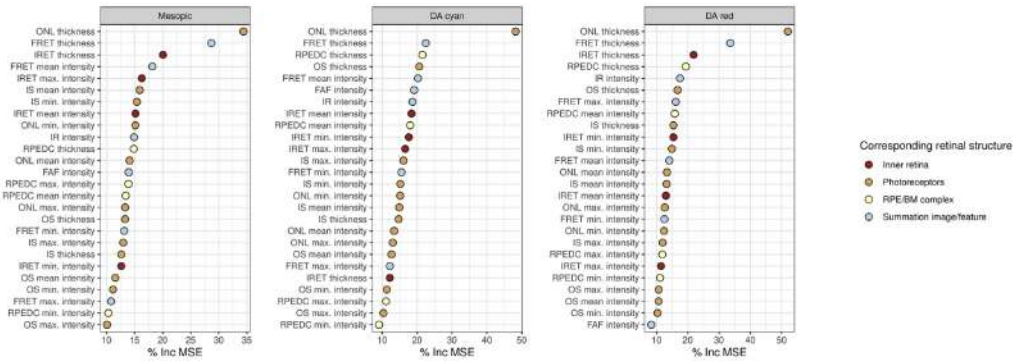

Figure 3.7: The dot plots show the permutation feature importance in terms of the % IncMSE. Notably, the HFL+ONL thickness constitutes the most important feature to predict retinal sensitivity in all three types of testing.

among the three types of testing. Slight levels of HFL+ONL thinning were associated with a marked DA cyan sensitivity loss, whereas mesopic sensitivity reduction was mostly observed in association with more severe degrees of HFL+ONL thinning (Figure 3.8).

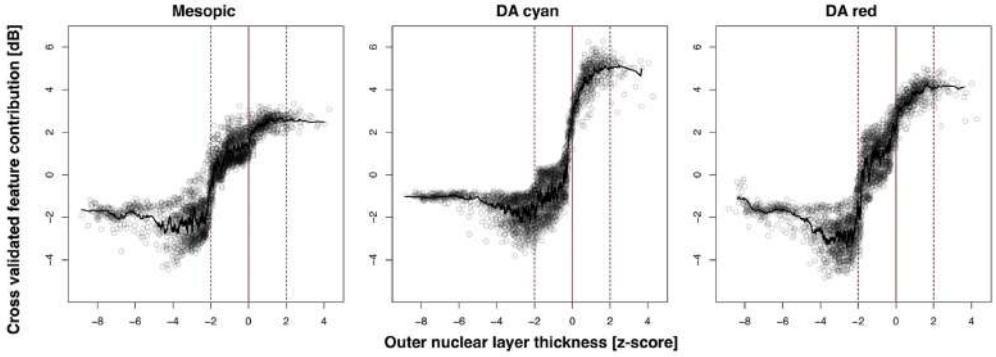

Figure 3.8: The plots show the feature contribution of HFL+ONL thickness toward the prediction of retinal sensitivity (i.e., the association after accounting for all other predictors). Slight degrees of HFL+ONL thinning are associated with marked DA cyan sensitivity loss. In comparison, mesopic sensitivity loss was observed in the context of more severe HFL+ONL thinning.

3.4 Prognostic Features of Overall Atrophy Progression[4]

3.4.1 Cohort Description

A total of 296 eyes of 201 patients (71 male [35.3%], 130 female [64.7%] patients) were included in this analysis. The average age at baseline was 72.20 ± 13.08 years. Most eyes presented with multifocal lesions (unifocal 42.2%, oligofocal [2 - 4 foci] 34.5%, and polyfocal [>4 foci] 23.3%). The mean square root progression rate was 0.31 mm per year.

3.4.2 Inter-Reader Reliability for Shape-Descriptive Factors

For the subset of 100 visits graded by two masked readers, the coefficients of repeatability (CoRs) were 0.20 mm for the square root area, 5.64 mm for the perimeter, 0.07 for the circularity, 1.03 mm for the $\text{Feret}_{\text{max}}$, 0.54 for the $\text{Feret}_{\text{min}}$, and 2.30 for the focality.(cf. Figure 2 in publication 4 [page 110*ff*]). A slightly worse inter-reader reliability was evident for measurements with greater absolute values with the exception of area and circularity measurements.

3.4.3 Prediction of Geographic Atrophy Progression Rates using Individual Shape-Descriptive Factors

For scenario 1 (leave-one-out cross validation on the patient level, "previously unknown patient" [i.e., no patient-specific intercepts and slopes]), univariable models allowed to predict future progression rates with an accuracy of (cross-validated R^2) 0.233 based on the $\text{Feret}_{\text{min}}$ diameter, 0.210 based on the square-root circularity, 0.098 based on the square-root perimeter, 0.088 based on the FAF phenotype, 0.056 based on the focality, 0.031 based on the $\text{Feret}_{\text{max}}$ diameter, and 0.003 based on the square-root lesion area.

Further, a model version reflecting the current inclusion criteria for ongoing clinical trials (typically: [square root] lesion area, FAF phenotype, and focality) was evaluated for the first scenario. The coefficient of determination ($R^2 = 0.150$) indicated that this version could explain 15% of the variability of future GA progression rates. A linear model including all features resulted in a cross-validated R^2 value of 0.244, indicating that these shape-descriptive factors (including the FAF phenotype) explained 24.4% of the variability of future GA progression.

For scenario 2 (leave-one-out cross validation on the visit level, "patient with previous clinical data available"), the model without any shape-descriptive factors (auto-correlation of prior progression rates with future progression rates) resulted in a coefficient of determination (R^2) of 0.185, indicating that previous progression rates explained 18.5% of the variability of future GA progression rates. The combined model with all features yielded a cross-validated R^2 of 0.391, indicating that

[4]This section constitutes a synopsis of the results of *Pfau M* and Lindner M* et al. Prognostic Value of Shape-Descriptive Factors for the Progression of Geographic Atrophy Secondary to Age-Related Macular Degeneration. Retina. 2019 Aug;39(8):1527-1540.* The original publication is attached as appendix (page 110*ff*).

the evaluated shape-descriptive factors (like the FAF phenotype) in conjunction with prior observation of the patient could explain 39.1% of the variability in future GA progression rates.

3.4.4 Correlation with Previously Reported Risk Factors

Evidently, the circularity varied markeldy in dependence of the FAF phenotype (Figure 3.9). Since the FAF phenotype (especially diffuse-trickling vs. non-trickling FAF phenotype) were shown to be prognostic for GA progression in prior publications (Holz et al., 2007), the analyses were repeated excluding eyes with the diffuse-trickling GA (cf. Supplemental Digital Content 4 in Pfau et al., 2018). To further confirm that the results are not determined by the disease severity, we conducted the same analysis stratified according to lesion dimensions (cf. Supplemental Digital Content 3 in Pfau et al., 2018). The results of these sub-analyses were overall similar to the main results.

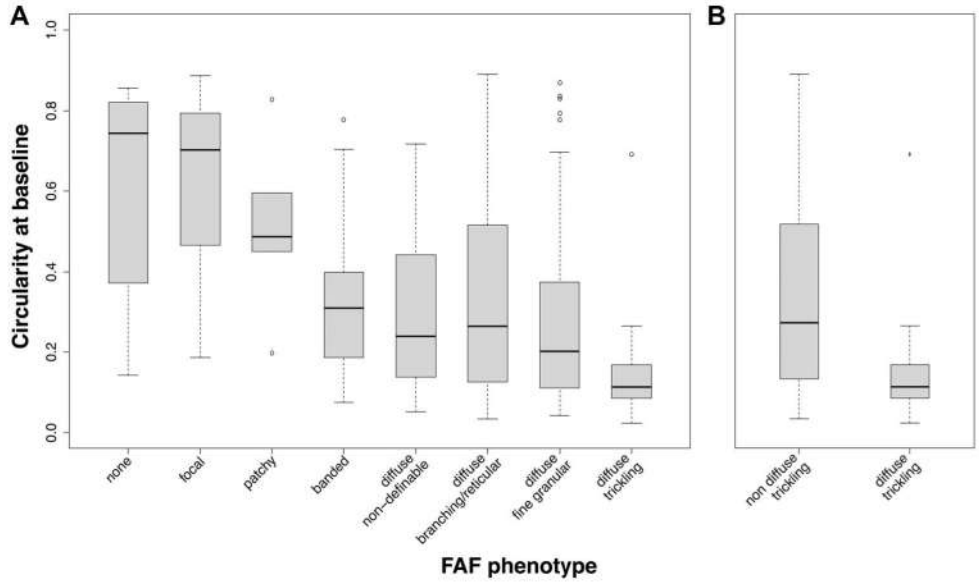

Figure 3.9: Circularity in dependence of the FAF phenotype. Notably, the diffuse-trickling FAF phenotype exhibits the lowest circularity given the typical multi-focal and multi-lobular configuration of GA in these eyes.

3.5 Inverse Association of Type 1 Neovascularization with Localized Atrophy Progression[5]

3.5.1 Cohort Description

A total of 98 eyes of 59 patients with an average age (± SD) of 76.60 ± 6.65 years with a median [IQR] follow-up of 1.17 years [1.01, 1.55] were included in this analysis. These eyes have been categorized as follows: seven eyes with RPE-atrophy and treatment-naïve quiescent CNV; ten eyes with RPE-atrophy and (former) exudative type 1 CNV; and a total of 81 eyes with RPE-atrophy with no signs of CNV (i.e., pure GA). Patients were excluded due to absence of RPE-atrophy (n=7), presence of fibrotic lesions or type two MNV membranes (n=7) or because of inadequate image quality (n=6).

RPE-atrophy lesion size and age at baseline did not differ significantly in dependence of the diagnostic subgroup (i.e., RPE-atrophy with treatment-naïve quiescent type 1 CNV, RPE-atrophy with exudative type 1 CNV, or RPE-atrophy with no evidence of CNV; cf. Table 2 in publication 5 [page 123*ff*]).

3.5.2 Validation of the Spatial Model for Future GA Progression

To confirm the goodness-of-fit of the (mixed effects) logistic regression model, patient-wise cross-validation was applied. The spatial overalp between predicted RPE-atrophy and observed RPE-atrophy was (Dice coefficient [95% CI]) 0.87 [0.85, 0.89], when considering all topographic locations, and 0.51 [0.47, 0.55], when considering only previously non-atrophic retina.

3.5.3 Association of Neovascularization and Localized RPE-Atrophy Progression

The point-wise (mixed effects) logistic regression model revealed that the follow-up time, distance to the RPE-atrophy boundary, eccentricity from the fovea as well as the horizontal position (temporal versus nasal retina) were significantly associated with the localized future RPE-atrophy progression (cf. Table 3 in publication 5 [page 123*ff*]).

Notably, the localized presence of treatment-naïve quiescent type 1 MNV was associated with markedly reduced odds for localized future RPE-atrophy progression (odds ratio [95% CI] of 0.21 [0.19, 0.24]; $P < 0.001$). Similarly, the localized presence of exudative type 1 MNV was associated with markedly reduced odds for localized future RPE-atrophy progression (0.46 [0.41, 0.51]; $P < 0.001$). The "eye-level" diagnosis of exudative type 1 MNV was additionally associated with a reduced RPE-atrophy progression in a "global" (i.e., spatially unspecific) manner (0.31 [0.18,

[5]This section constitutes a synopsis of the results of *Pfau M et al. Type 1 Choroidal Neovascularization Is Associated With Reduced Localized Progression of Atrophy in Age-Related Macular Degeneration. Ophthalmol Retina. 2020 Mar;4(3):238-248.* The original publication is attached as appendix (page 123*ff*).

0.53]; $P < 0.001$). A marginal effects plot - limited to the immediate junctional-zone surrounding the RPE-atrophy (0.5° [approx. 145 μm]) - underscores the pronounced association of treatment-naïve quiescent and exudative type 1 MNV with a reduced probability of future RPE-atrophy progression (Figure 3.10).

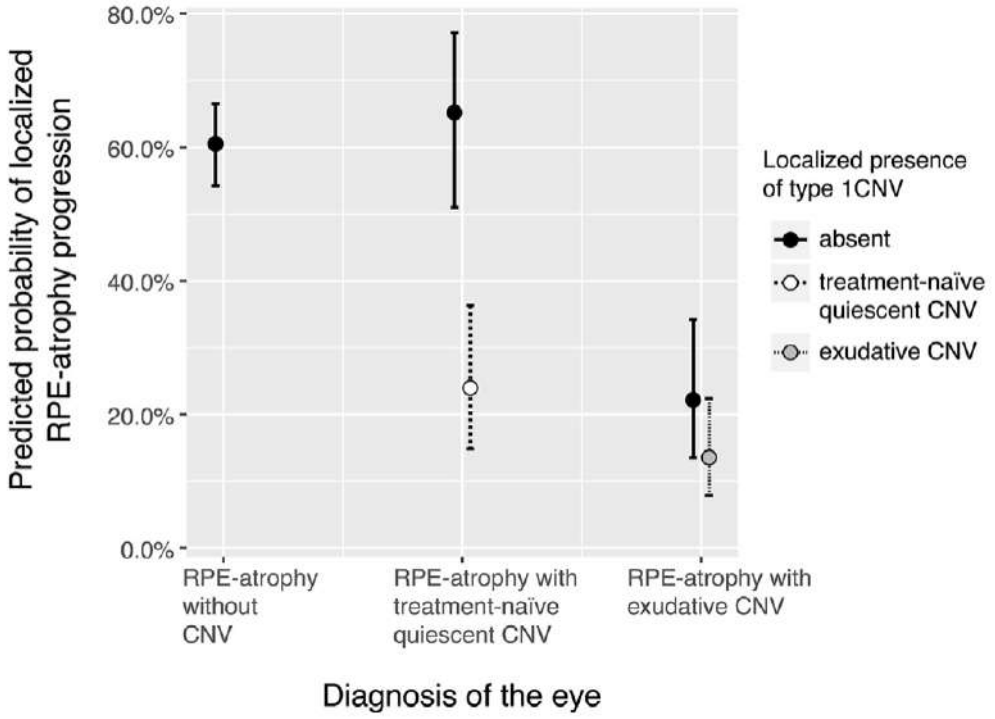

Figure 3.10: Probability of localized RPE-atrophy progression in the junctional zone. The marginal effects plot shows the predicted marginal probabilities and 95% CIs for the localized progression of RPE-atrophy in the junctional-zone (0.5° [approx. 145 μm] boundary of RPE-atrophy) in dependence of the per-eye diagnosis (x-axis) and the point-wise presence/absence of treatment-naïve quiescent and exudative type 1 MNV (line type).

3.5.4 Long-Term Association between MNV and Reduced Localized RPE-Atrophy Progression

For four eyes (three patients) long-term imaging information was available that had been collected in the context of the DSGA 1 study prior to the baseline of this investigation (P1: 7 years and 6 month, P2: 4 years and 6 weeks, P3: 5 years). Though, no OCTA information was available for all these earlier study visits, there was evidence of quiescent type 1 MNV or exudative type 1 MNV based on SD-OCT ('double layer signal') and FA (stippled hyperfluorescence) in these patients (Figure 4.2 and Figure 5 in publication 5 [page 123*ff*]). Qualitatively, RPE-atrophy progression in regions of quiescent type 1 MNV or exudative type 1 CNV was markedly reduced in these patients with a follow-up of multiple years.

Chapter 4

Discussion

This thesis highlighted a new approach with regard to perimetry test-patterns to probe function in GA. These so-called *"patient-tailored"* perimetry test-patterns allowed to probe in detail the function in the outer junctional zone, as well as inner junctional zone. The subsequent machine-learning-based analyses highlighted the close correlation between retinal structure and function. In addition, the last two publications of this thesis defined prognostic features for overall GA progression and demonstrated a marked association of type 1 MNV with reduced localized RPE atrophy progression. As discussed in the following sections, these results may inform future therapeutic approaches (cf. section 4.8.1) and have implications for the design of clinical trials (cf. section 4.8.2).

4.1 Retinal Sensitivity in Geographic Atrophy

4.1.1 Retinal Sensitivity in the Junctional Zone

The (outer) junctional zone of GA has been previosuly described as a spatial sequence of degenerative changes, that may be considered as a spatial surrogate for degeneration over time (Li et al., 2018; J. P. Sarks et al., 1988; Zanzottera et al., 2016). In this region from 500 μm to 100 μm from the GA boundary, a distinct progression of RPE dysmorphia associated with thickening of BLamD, as well as increase of CC loss could be evidenced in recent histopathologic studies (Biesemeier et al., 2014; Li et al., 2018; Zanzottera et al., 2016).

Overall, the here observed gradual sensitivity loss toward the GA boundary is very much consistent with these histopathological reports. Specifically, mesopic sensitivity loss was rather uniform for test points 1.29° (375 μm) or more distal to the GA boundary (cf. Figure 3.2), which parallels the zone of ONL dyslamination, and cone photoreceptor inner segment myoid shortening (Li et al., 2018).

4.2 Rod versus Cone Degeneration in the Junctional Zone

DA cyan sensitivity loss as a measure of rod function was overall much more severe (cf. Figure 3.2), which may either be attributable to structural degeneration of rod

photoreceptors and/or impairment of the canonical visual cycle.

Multiple previous psychophysical and histopathologic studies have evidenced an increased vulnerability of rod photoreceptor in AMD. Specifically, a hallmark histopathologic study by Christine A. Curcio showed that the foveal cone mosaic is typically similar in patients with AMD compared to that of age-matched controls, whereas the parafovea exhibits severe rod photoreceptor loss (Curcio et al., 1996). Other histopathologic studies confirmed the notion that rod degeneration precedes cone degeneration, especially in proximity to AMD-associated lesion such as atrophic and fibrotic scars (Shelley et al., 2009). Psychophysically, selective (or more severe) rod dysfunction could be evidenced comparing steady-state DA cyan sensitivity loss against light-adapted sensitivity loss (Owsley et al., 2000). This observation was later reproduced by multiple groups and was shown to be associated to some degree with the extent of RPD (Flynn et al., 2018; Pfau et al., 2018; Steinberg et al., 2015; Tan et al., 2018). Moreover, discriminant validity (between AMD stages) and ability to detect change (K. G. Chen et al., 2019; Flamendorf et al., 2015; Owsley et al., 2016), as well as predictive validity for future AMD incidence could be established for dark adaptometry (Owsley et al., 2016).

The here presented study now adds a detailed description of photoreceptor dysfunction in the junctional zone of GA to the literature. Interestingly, the relationship between mesopic dysfunction and DA cyan sensitivity loss was non-linear cf. Figure 3.2, lower right panel). Mesopic dysfunction was only observed in conjunction with DA cyan sensitivity loss, however, DA cyan sensitivity loss could also be evidenced in presence of normal mesopic sensitivity. Careful extrapolation of these cross-sectional findings is supportive of the notion that rod degeneration precedes cone degeneration, even within the small scale of the junctional zone of GA (cf. Section 4.8.1 below).

4.3 Sensitivity within Areas of Geographic Atrophy

Minimal residual retinal sensitivity within areas of GA has been previously reported but not linked the corresponding retinal microstructure. In 1988, Sunness and coworkers reported with a custom-built fundus camera stimulator based on a modified Zeiss 308 fundus camera, that retinal sensitivity may be observed at small areas of atrophy 'comparable to the size of drusen' (Sunness et al., 1988).

By extension, we now studied systematically the sensitivity in the inner junctional zone of GA. The results indicate that mesopic and DA red sensitivity measurements may indeed not be purely explained by patient-specific false-positive response rates or other reliability indices (e.g., fixation stability with regard to inaccurate stimulus placement). Biologically, this is plausible, since the cone-specific visual cycle is independent of the RPE (J. S. Wang and Kefalov, 2011). Residual function was mainly evident in conjunction with residual or bridging HFL+ONL. According to histopathologic studies, residual or bridging HFL+ONL constitutes mostly dyslaminated HFL, but residual photoreceptor islands with presence of residual RPE (also termed open ORTs) may also be present. In addition, to the presence of degenerative cone photoreceptor cell bodies and nuclei (cf. Figure 6 in Li et al., 2018), opsin redistribution to cone cell bodies, axons, or axon terminals has been reported,

which could explain the observed residual sensitivity despite of the lack of OS in SD-OCT (Johnson et al., 2003; Shelley et al., 2009).

Of note, the differentiation between photoreceptor islands (without regularly arranged IS and OS) and dyslaminated HFL is likely not possible with SD-OCT. This may explain the rather wide standard error of the estimate of sensitivity in regions with HFL+ONL. Possibly, *in vivo* fluorescence lifetime ophthalmoscopy allows for such a differentiation between dyslaminated HFL and photoreceptor islands (Dysli et al., 2017). Using this technique, an 'intermediate lifetime border' within GA has been described, which may be indicative of visual cycle by-products that would support the hypothesis of remnant visual function (Dysli et al., 2016).

4.4 Determinants of Retinal Sensitivity

The machine-learning-based analysis of structure function correlation highlighted the close association between retinal microstructure and function. By extension, this approach could also be applied for mapping of "inferred sensitivity" across the whole imaged retina as shown in Figure 4.1. This type of map features many of the expected characteristics, which underscores the validity of the predictions. This includes a central DA cyan scotoma (given the central rod-free area) and a junctional zone of GA with predominant DA cyan sensitivity loss.

Interestingly, the HFL+ONL constituted the most important layer for all three types of sensitivity predictions. In an idealized model of isolated photoreceptor degeneration, the loss of light sensitivity would be proportional to the number of surviving photoreceptors and the length of their outer segments (S. G. Jacobson et al., 2005). In a transgenic rat model for autosomal dominant retinitis pigmentosa, it was previously shown that both of these parameters correlate to the ONL thickness (Machida et al., 2000). Thus, it is plausible from a biological view that the HFL+ONL constituted the most important layer for the predictions. Moreover, the other, thinner photoreceptor layers such as IS and OS are relatively susceptible to sub-optimal segmentation ('feature noise'), which typically results in a lesser feature importance in predictive models.

Further, the feature contribution plots (cf. Figure 3.8) highlighted that HFL+ONL thickening - a finding previously also reported in the setting of intermediate AMD (Sadigh et al., 2013) - was not associated with dysfunction. In contrast, HFL+ONL thinning were strongly associated with loss of retinal sensitivity in all three types of testing. Especially DA cyan sensitivity loss was evident for even slight degrees of HFL+ONL thinning as compared to DA mesopic sensitivity loss, which was mostly evident for loci with more severe degrees of HFL+ONL thinning. Again, this is compatible with histopathologic studies evidencing predominant loss of rod photoreceptors in proximity to AMD related lesions such as RPE atrophy and/or fibrovascular scars (Curcio et al., 1996; Shelley et al., 2009).

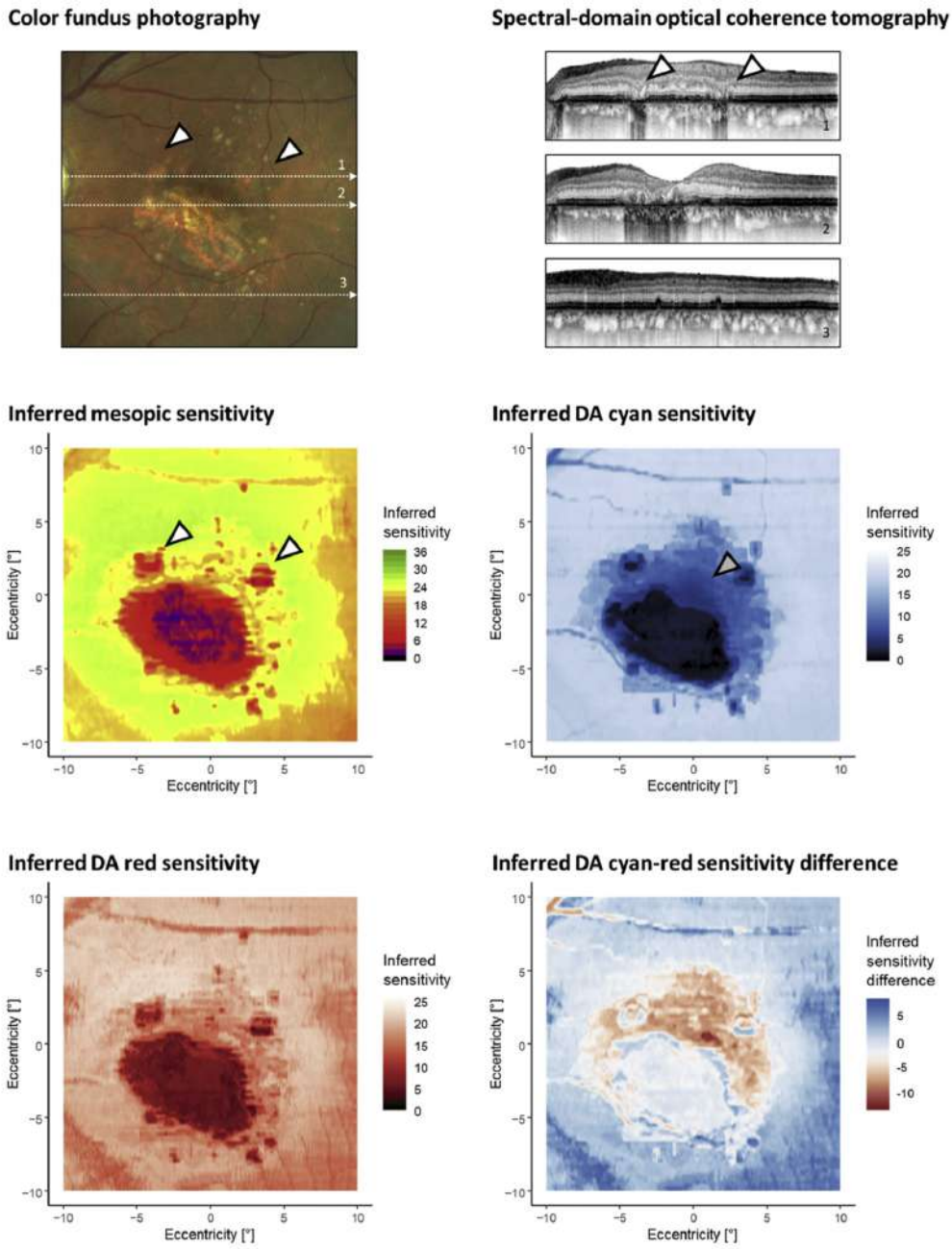

Figure 4.1: Mapping of "inferred sensitivity". The prediction of retinal sensitivity in this patients exhibits many of the expected key features. The white, dashed lines in the color fundus photography image indicate the SD-OCT B-scan positions. The model adequately predicted the functional loss for the two small foci of GA (white arrowheads). The prediction of DA cyan testing featured a central scotoma as expected given the central rod-free area (gray arrowhead). The sensitivity maps were slightly smoothed (median filtering, window: 3 px × 3 px).

4.5 Factors Associated with Accelerated Atrophy Progression

Inclusion criteria clinical trials for clinical trials encompass typically the FAF phenotype and the lesion size (e.g., NCT02247479, NCT02247531, NCT02087085). In

conjunction, these criteria allow to separate slow from medium and fast progressing lesions (Fleckenstein et al., 2018; Holz et al., 2007). Using color fundus photography based annotations, it has later been shown that the circularity is prognostic of future atrophy progression (Domalpally et al., 2013). By extension, we have now assessed in detail the prognostic value for a wide panel of shape-descriptive factors.

Interestingly, the minimum caliper diameter ($\text{Feret}_{\text{min}}$) was in the single factor models the most prognostic feature explaining up to 23.3% of the variability in progression rates in previously unknown patients. In conjunction with prior progression rates, the circularity was the most prognostic feature allowing to explain 37.9% of the variability in progression rates. Both of these R^2 values exceed the variability explained by the FAF phenotype and the lesion size.

GA progresses mostly in a linear manner along the lesion radius, i.e. perpendicular to the GA boundary (Feuer et al., 2013; Fleckenstein et al., 2010; Shen et al., 2018). Accordingly, square-root transformation of the lesion area is commonly used to obtain linear progression rates (Feuer et al., 2013; Shen et al., 2018). This also explains the high prognostic values a imaging features related to the extension of the lesion boundary (i.e., perimeter, and circularity).

Besides of imaging features, genetic, epigenetic, environmental, and demographic factors might also be prognostic for GA progression rates. The marked autocorrelation of former with future GA progression rates as observed here and in a previous study (Sunness et al., 2007), is suggestive of such time-invariant patient characteristics. However, in previous study combining data from AREDS and FAM, *ARMS2* rs10490924, and *C3* rs2230199, and fellow eye status explained only 7.2% of the observed inter-individual variability in GA progression rates (Grassmann et al., 2015).

The approach of using shape-descriptive factors to explain future progression rates of RPE atrophy has now been validated in our group in the context of Stargardt disease (Müller, Pfau, Treis, et al., 2020), and retinopathy secondary to Maternally Inherited Diabetes and Deafness (MIDD) (Müller, Treis, et al., 2020) as well.

4.6 Inverse Association of Type 1 Neovascularization with Atrophy Progression

Previous studies reported qualitatively and semi-quantitatively that quiescent or exudative type 1 MNV are associated with a reduced localized progression of RPE atrophy (Christenbury et al., 2018). This study now underscores this observation in a quantitative manner. As shown for the exemplary patients in Figure 4.2, the magnitude of the association of type 1 MNV with reduced localized RPE atrophy progression is clinically meaningful.

Biologically, two potentially synergistic mechanisms may confer a protective effect of type 1 MNV on RPE atrophy progression. Histopathologic studies have identified a lipophilic interchange barrier at the level of BrM as a characteristic of AMD Curcio, 2018b; Pauleikhoff et al., 1990. Further, CC breakdown exceeding the boundaries of GA has been evidenced *in vivo* using *OCTA* (Müller et al., 2018; Nassisi et al., 2019; Thulliez et al., 2019), as well as histopathologically (Biesemeier

et al., 2014; Li et al., 2018). Based on the anatomical location of type 1 MNV in the sub-RPE–basal lamina space, type 1 MNV bypasses the interchange barrier at the level of BrM and may compensate for the CC breakdown (L. Chen et al., 2020). Indeed, in a histopathologic study of non-exudative type 1 MNV, formation of capillary-like neovessels with fenestrations and caveolae resembling native CC supporting the overlaying RPE has been reported (L. Chen et al., 2020). In conjunction these results suggest, that cessation of exudation with a remnant type 1 membrane may constitute the optimal treatment target in anti-VEGF therapy. On a similar note, it was recently shown that tolerating some exudative activity in the form of subtle subretinal fluid results in a similar outcome as a treatment aimed at resolving all subretinal fluid (Guymer et al., 2019). The results have also further implications regarding potential future therapeutic targets (cf. Section 4.8.1).

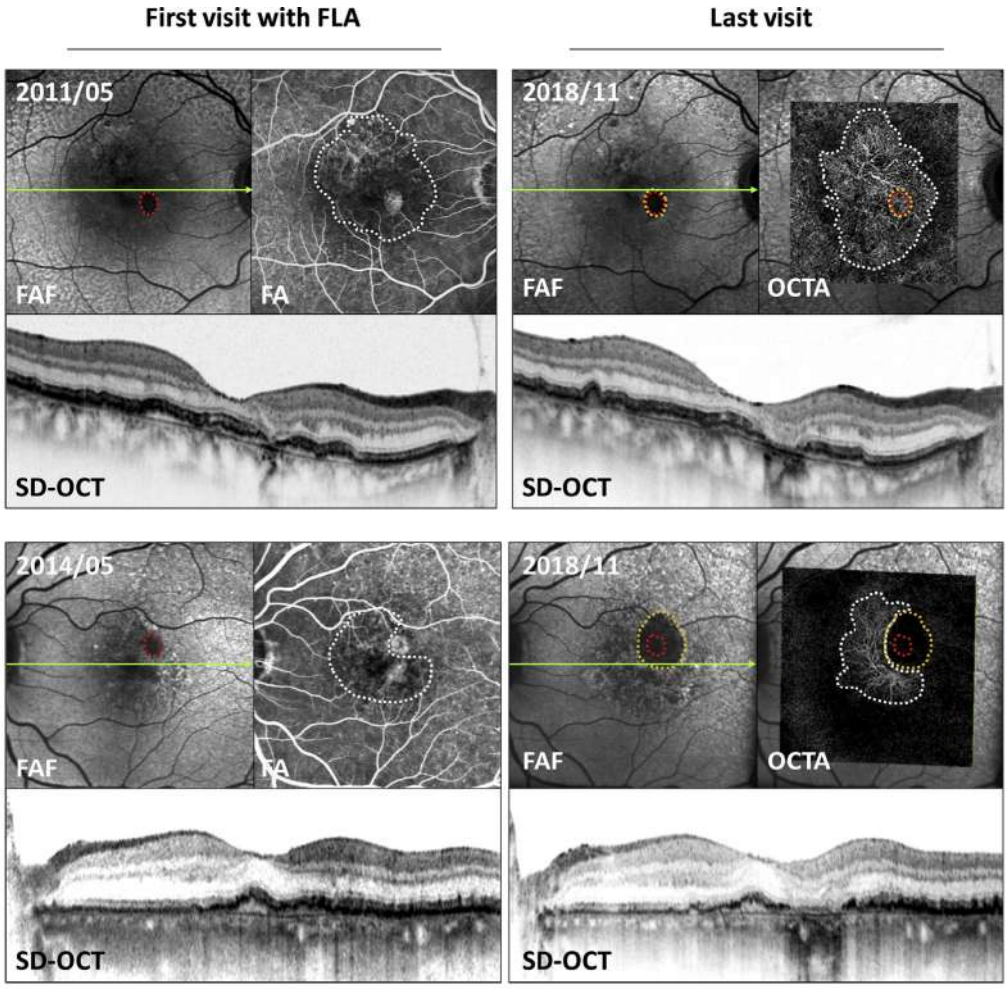

Figure 4.2: The figure shows multimodal imaging data of two patients with non-exudative type 1 MNV and RPE atrophy. The white dashed lines denote the area of non-exudative type 1 MNV. The red dashed line denote RPE atrophy at baseline and the yellow dashed lines enote RPE atrophy at the last visit. In the first patient (upper row), the RPE atrophy lesion embedded within a region of non-exudative type 1 MNV appears to almost not progress. In the second patient (lower row), RPE atrophy apprears to progress much more rapidly distal to the non-exudative type 1 MNV than toward it.

4.7 Limitations

Multiple limitations of the here presented studies must be considered.

The analysis of the sensitivity in the junctional zone in GA is based on a relatively small number of subjects and cross-sectional. Nevertheless, it constitutes the largest study with mesopic and DA two-color testing as well as an intra-session retest examination. Further, no cone-specific test setting (i.e, photopic white-on-white or red-on-white testing) was available for the S-MAIA device or any other FCP device at the time of the study. Recently, a FCP device allowing for photopic testing became available (Pfau, Jolly, et al., 2020).

The patient-tailored test-patterns were designed for probing of the retinal sensitivity in the outer junctional zone. Accordingly, the number of test points available for the analysis of sensitivity in the inner junctional zone was limited. Conclusions for ORTs may not be drawn with certainty due to the limited number of test points co-localizing with ORTs. Further, hyperreflective spots internal to BrM, which may represent migrated RPE cells, were visible in areas of atrophy (Li et al., 2018). High resolution functional testing (in terms of stimulus size), such as adaptive optics scanning laser ophthalmoscopy-based perimetry (Harmening et al., 2014), would be required to examine, whether these foci affect retinal function.

For the machine learning-based prediction of retinal sensitivity, it must be noted that the test-retest MAE of perimetry testing was slightly smaller than the MAE between predictions and observations. Accordingly, a larger sample size may be needed to maximize the prediction accuracy. In addition, a deep-learning instead of a machine-learning model, as recently applied in the context of macular telangiectasia type 2 (Kihara et al., 2019), could have (potentially) provided a slightly better prediction accuracy. However, we elected a machine-learning model in consideration of interpretability (cf. Figure 3.8).

Regarding GA progression, more recent and accurate models became available to predict GA progression incorporating SD-OCT information GA (Niu et al., 2016). Moreover, multiple studies underscore that CC flow signal voids in OCTA are prognostic for future GA progression (Müller et al., 2018; Nassisi et al., 2019; Thulliez et al., 2019). An analysis that includes all of these potentially prognostic features followed by variable selection (e.g., through least absolute shrinkage and selection operator [lasso] regression) will be needed to identify the most important prognostic features.

The association of type 1 MNV with localized atrophy progression was studied in a rather binary manner by classifying pixels as overlaying / not-overlaying type 1 MNV. However, it is clinically evident, that the vascular density and patterns within type 1 MNV vary greatly (von der Emde et al., 2020). To further examine the potential protective effect of type 1 MNV against RPE atrophy progression, the biological gradient of the relationship warrants investigation. Hypothetically, the protective effect is a function of the vascular density of the neovessels.

4.8 Implications and Future Directions

The following section briefly highlights implications of the here presented results for future therapeutic approaches and for the design of clinical trials. Some of the below mentioned implications (e.g., "point-of-no-return") are based on careful extrapolation of the here presented results and previous research. Further research will be needed to confirm or disprove these hypotheses.

4.8.1 Implications for the Therapy of Age-Related Macular Degeneration

"Spare the Rods, Save the Cones"

The expression "Spare the Rods, Save the Cones" has been coined in the context AMD by Christine A. Curcio, Cynthia Owsley, and Gregory R. Jackson (Curcio et al., 2000). The authors based their proposed therapeutic strategy on histopathologic evidence (Curcio and Allen, 1993; Curcio et al., 1996), as well as psychophysical evidence (Jackson et al., 1999; Owsley et al., 2000), which demonstrated that rod degeneration precedes cone degeneration in AMD. The here shown non-linear relationship between DA cyan sensitivity loss (which could be observed in isolation) and mesopic sensitivity loss (which was only observed in conjunction with DA cyan sensitivity loss) is indeed indicative of a temporal sequence between rod and subsequent cone degeneration (cf. Figure 3.2 lower right panel). Cone sensitivity loss could only be observed for loci with a rod sensitivity loss of approx. 16 dB or more (i.e., deflection point of the non-linear relationship). Interestingly, this exact non-linear relationship between rod and cone sensitivity loss with the same deflection point is not only also evident in other BrM diseases such as Pseudoxanthoma elasticum (Hess et al., 2020), but also in unrelated diseases such as *RHO*-associated autosomal dominant retinitis pigmentosa (cf. Figure 2B in Cideciyan et al., 1998). In conjunction, this suggests that the mechanisms leading to secondary cone degeneration are overall disease unspecific (Aït-Ali et al., 2015). Thus, disease-specific strategies to prevent early rod photoreceptor degeneration or disease-unspecific strategies to prevent secondary cone degeneration may allow to spare central cone vision in patients with AMD (Curcio et al., 2000).

4.8.2 Implications for Clinical Trials

Retinal Sensitivity as Functional Outcome Measure

Previously, conventional perimetry patterns such as the 10-2 grid have been employed to follow GA progression (Meleth et al., 2011). However, the ability to detect change over time was rather limited. While GA may progress through *de-novo* foci, progression of GA occrus predimonalty in the junctional zone in an "appositional growth"-like manner (Fleckenstein et al., 2010). Therefore, rectilinear spaced test points with a distance of 2° to each other, are sub-optimal to capture the progression of GA (median of 106.90 μm/y or approx. 0.37°/y, cf. Fleckenstein et al., 2010). A prospective, longitudinal study, which is currently ongoing, will be needed to demonstrate the advantage of patient-tailored test-patterns.

Inferred Sensitivity as Surrogate Outcome

As shown in Figure 4.1, spatial mapping of inferred sensitivity exceeds the limitations of psychophysical testing in terms of spatial resolution as well as area covered. Criteria for the "evidence for surrogacy" have been established by the International Conference on Harmonization (ICH) Guidelines on Statistical Principles for Clinical Trials (International Conference on Harmonisation E9 Expert Working Group, 1999). This includes *"(i) the biological plausibility of the relationship, (ii) the demonstration in epidemiologic studies of the prognostic value of the surrogate for the clinical outcome and (iii) evidence from clinical trials that treatment effects on the surrogate correspond to effects on the clinical outcome"* (International Conference on Harmonisation E9 Expert Working Group, 1999). As discussed above (cf. Section 4.4), the feature importance values are indicative of biological plausibility. The second criterion is also met, given that "inferred sensitivity" may be equated to function as opposed to other conventional surrogate endpoints such as intra-ocular pressure in glaucoma. For the last criterion, a prospective study comparing "inferred sensitivity" and measured sensitivity in the context of a given treatment will be needed.

Area of Atrophy as Structural Outcome Measure

Our data supports the application of FAF-based quantification of GA in AMD as structural outcome measure in clinical trails as previously proposed Holz et al., 2007. The current work highlights that the boundary of GA constitutes a 10- to 15-fold change in retinal sensitivity. Even for regions with residual HFL+ONL within GA, the boundary delineates an approximately a 5 dB (i.e., three-fold) drop in sensitivity.

"Point-of-no-return"

In recent years, therapeutic trials for GA were characterized by rather brief follow-up periods (e.g., NCT02247479, NCT02247531, NCT02087085). However, histopathologic (Biesemeier et al., 2014; Li et al., 2018; J. P. Sarks et al., 1988; Zanzottera et al., 2016), OCTA (Müller et al., 2018; Nassisi et al., 2019; Thulliez et al., 2019) and the here presented functional data jointly demonstrate severe alterations of the CC and outer retina in the immediate junctional zone of GA (within 375 μm of the RPE atrophy boundary). In consideration of the lateral spread of GA (median 106.90 mm/y, Fleckenstein et al., 2010), it is conceivable that the rate of GA progression is partially predetermined for 1 to 3 years. Accordingly, significantly longer follow-up periods seem warranted to assess treatment effects on GA progression beyond this 375 μm boundary (i.e., follow-up of 4 years or longer). Alternatively, one could also consider degenerative processes distal to the boundary of GA, such as progressive *"macula-wide"* thinning of the HFL+ONL, as outcome measure (Pfau, von der Emde, et al., 2020).

Chapter 5

Summary

This thesis summarizes five studies based on data collected prospectively by the author in the context of the Directional Spread in Geographic Atrophy 2 (DSGA 2, ClinicalTrials.gov: NCT02051998, PI: M. Fleckenstein) study, as well as an ancillary FCP study and a normative data study.

First, a new approach to perimetry with *'patient-tailored'* test-patterns could be established, which allows to test retinal sensitivity with high spatial-resolution in the junctional zone of GA. Using DA two-color perimetry, it could be demonstrated that rod photoreceptor dysfunctions exceeds cone photoreceptor dysfunction in this defined region. Moreover, relative uniformity of the retest-reliability, even in close proximity to the GA boundary, highlights that these *'patient-tailored'* perimetry patterns could be applied in clinical trials to monitor GA progression.

Second, structure-function analysis was applied to investigate the potential association of residual (bridging) HFL+ONL within areas of RPE atrophy as well as ORTs with retinal sensitivity. It was shown that measured sensitivities within the inner junctional zone of GA may not be purely explained by patient-specific false-positive response rates or other reliability indices. Specifically, residual HFL+ONL was associated with residual mesopic and DA red sensitivity. This is indicative of a *'therapeutic window'* for cell replacement therapeutics. Moreover, it defines a baseline level of function that a given cell replacement intervention must surpass to demonstrate efficacy.

Third, it was demonstrated that outer retinal microstructure correlates closely to retinal function. By using a machine-learning approach, a plethora of imaging features (instead of few 'hand-crafted' features) could be included, despite of multicollinearity (correlation among the input variables). We were able to predict retinal sensitivity in patients with GA with an accuracy that almost matches the retest-variability of fundus-controlled perimetry testing. Moreover, the machine-learning approach highlighted the relevance of HFL+ONL as predictor of retinal sensitivity. While loss of rod sensitivity could already be evidenced in association with slight degrees of HFL+ONL thinning, loss of mixed cone and rod function (mesopic sensitivity) was mostly evident in presence of more severe HFL+ONL thinning. This cross-sectional observation is suggestive of a temporal sequence of rod and subsequent cone photoreceptor degeneration.

Fourth, this thesis underscores that the FAF phenotype as indicator of widespread outer retinal and RPE alterations and shape-descriptive factors such as the lesion circularity are prognostic for future RPE atrophy progression. Moreover,

the analysis confirmed that the patient-specific prior progression rate constitutes the most important predictive variable. Thus, addition of prior observations would constitute a meaningful addition to clinical trial inclusion criteria.

Fifth, this thesis examined the association of type 1 MNV with a reduced localized progression of RPE atrophy. In contrast to prior observational and semi-quantitative analyses, the here presented analysis allowed to formally test the hypothesis that treatment-naïve quiescent type 1 MNV is associated with a reduced localized progression of RPE atrophy. These *in vivo* results highlight the relevance of the BrM-CC complex for the integrity of the overlying RPE. Potential therapeutic approaches for GA including strategies to enhance sub-RPE perfusion or targeting the impaired interchange across BrM are supported by these results.

Chapter 6

References

Aït-Ali, N., Fridlich, R., Millet-Puel, G., Clérin, E., Delalande, F., Jaillard, C., Blond, F., Perrocheau, L., Reichman, S., Byrne, L. C., Olivier-Bandini, A., Bellalou, J., Moyse, E., Bouillaud, F., Nicol, X., Dalkara, D., Van Dorsselaer, A., Sahel, J. A., & Léveillard, T. (2015). Rod-derived cone viability factor promotes cone survival by stimulating aerobic glycolysis. *Cell*, *161*(4), 817–832. https://doi.org/10.1016/j.cell.2015.03.023

Bates, D., Mächler, M., Bolker, B., & Walker, S. (2015). Fitting Linear Mixed-Effects Models Using lme4. *Journal of Statistical Software; Vol 1, Issue 1 (2015)*. https://www.jstatsoft.org/v067/i01%20http://dx.doi.org/10.18637/jss.v067.i01

Bearelly, S., Chau, F. Y., Koreishi, A., Stinnett, S. S., Izatt, J. A., & Toth, C. A. (2009). Spectral Domain Optical Coherence Tomography Imaging of Geographic Atrophy Margins. *Ophthalmology*, *116*(9), 1762–1769. https://doi.org/10.1016/j.ophtha.2009.04.015

Biesemeier, A., Taubitz, T., Julien, S., Yoeruek, E., & Schraermeyer, U. (2014). Choriocapillaris breakdown precedes retinal degeneration in age-related macular degeneration. *Neurobiology of Aging*, *35*(11), 2562–2573. https://doi.org/10.1016/j.neurobiolaging.2014.05.003

Bland, J. M., & Altman, D. G. (1999). Measuring agreement in method comparison studies. *Statistical Methods in Medical Research*, *8*(2), 135–160. https://doi.org/10.1177/096228029900800204

Capuano, V., Miere, A., Querques, L., Sacconi, R., Carnevali, A., Amoroso, F., Bandello, F., Souied, E. H., & Querques, G. (2017). Treatment-Naïve Quiescent Choroidal Neovascularization in Geographic Atrophy Secondary to Nonexudative Age-Related Macular Degeneration. *American Journal of Ophthalmology*, *182*, 45–55. https://doi.org/10.1016/j.ajo.2017.07.009

Carnevali, A., Cicinelli, M. V., Capuano, V., Corvi, F., Mazzaferro, A., Querques, L., Scorcia, V., Souied, E. H., Bandello, F., & Querques, G. (2016). Optical Coherence Tomography Angiography: A Useful Tool for Diagnosis of Treatment-Naïve Quiescent Choroidal Neovascularization. *American Journal of Ophthalmology*, *169*, 189–198. https://doi.org/10.1016/j.ajo.2016.06.042

Chen, K. G., Alvarez, J. A., Yazdanie, M., Papudesu, C., Wong, W. T., Wiley, H. E., Keenan, T. D., Chew, E. Y., Ferris, F. L., & Cukras, C. A. (2019). Longitudinal Study of Dark Adaptation as a Functional Outcome Measure for Age-Related Macular Degeneration. *Ophthalmology*, *126*(6), 856–865. https://doi.org/10.1016/j.ophtha.2018.09.039

Chen, L., Messinger, J. D., Sloan, K. R., Swain, T. A., Sugiura, Y., Yannuzzi, L. A., Curcio, C. A., & Freund, K. B. (2020). Nonexudative Macular Neovascularization Supporting Outer Retina in Age-Related Macular Degeneration: A Clinicopathologic Correlation. *Ophthalmology*. https://doi.org/10.1016/j.ophtha.2020.01.040

Chew, E. Y., Clemons, T. E., SanGiovanni, J. P., Danis, R., Ferris, F. L., Elman, M., Antoszyk, A., Ruby, A., Orth, D., Bressler, S., Fish, G., Hubbard, B., Klein, M., Chandra, S., Blodi, B., Domalpally, A., Friberg, T., Wong, W., Rosenfeld, P., … Sperdut, R. (2013). Lutein + zeaxanthin and omega-3 fatty acids for age-related macular degeneration: The Age-Related Eye Disease Study 2 (AREDS2) randomized clinical trial. *JAMA - Journal of the American Medical Association*, *309*(19), 2005–2015. https://doi.org/10.1001/jama.2013.4997

Christenbury, J. G., Phasukkijwatana, N., Gilani, F., Freund, K. B., Sadda, S., & Sarraf, D. (2018). Progression of macular atrophy in eyes with type 1 neovascularization and age-related macular degeneration receiving long-term intravitreal anti-vascular endothelial growth factor therapy: An optical coherence tomographic angiography analysis. *Retina*, *38*(7), 1276–1288. https://doi.org/10.1097/IAE.0000000000001766

Cideciyan, A. V., Hood, D. C., Huang, Y., Banin, E., Li, Z. Y., Stone, E. M., Milam, A. H., & Jacobson, S. G. (1998). Disease sequence from mutant rhodopsin allele to rod and cone photoreceptor degeneration in man. *Proceedings of the National Academy of Sciences of the United States of America*, *95*(12), 7103–7108. https://doi.org/10.1073/pnas.95.12.7103

Colijn, J. M., Buitendijk, G. H., Prokofyeva, E., Alves, D., Cachulo, M. L., Khawaja, A. P., Cougnard-Gregoire, A., Merle, B. M., Korb, C., Erke, M. G., Bron, A., Anastasopoulos, E., Meester-Smoor, M. A., Segato, T., Piermarocchi, S., de Jong, P. T., Vingerling, J. R., Topouzis, F., Creuzot-Garcher, C., … Zwiener, I. (2017). Prevalence of Age-Related Macular Degeneration in Europe: The Past and the Future. *Ophthalmology*, *124*(12), 1753–1763. https://doi.org/10.1016/j.ophtha.2017.05.035

Colijn, J. M., Verzijden, T., Meester-Smoor, M. A., Klaver, C. C., Colijn, J. M., Demirkan, A., Verzijden, T., Meester-Smoor, M. A., Ahmad, S., van Duijn, C. M., Klaver, C. C., den Hollander, A. I., Kersten, E., Hoyng, C. B., Klaver, C. C., Cougnard-Grégoire, A., Merle, B. M., Korobelnik, J. F., Delcourt, C., … Zumbansen, M. (2019). Increased High-Density Lipoprotein Levels Associated with Age-Related Macular Degeneration: Evidence from the EYE-RISK and European Eye Epidemiology Consortia. *Ophthalmology*, *126*(3), 393–406. https://doi.org/10.1016/j.ophtha.2018.09.045

Curcio, C. A. (2018a). Antecedents of soft drusen, the specific deposits of age-related macular degeneration, in the biology of human macula. *Investigative Ophthalmology and Visual Science*, *59*(4), AMD182–AMD194. https://doi.org/10.1167/iovs.18-24883

Curcio, C. A. (2018b). Soft drusen in age-related macular degeneration: Biology and targeting via the oil spill strategies. *Investigative Ophthalmology and Visual Science*, *59*(4), AMD160–AMD181. https://doi.org/10.1167/iovs.18-24882

Curcio, C. A., & Allen, K. A. (1993). Aging of the Human Photoreceptor Mosaic: Evidence for Selective Vulnerability of Rods in Central Retina. *Investigative ophthalmology & visual science*, *34*(12), 3278–3296.

Curcio, C. A., McGwin, G., Sadda, S. R., Hu, Z., Clark, M. E., Sloan, K. R., Swain, T., Crosson, J. N., & Owsley, C. (2020). Functionally validated imaging endpoints in the Alabama study on early age-related macular degeneration 2 (ALSTAR2): design and methods. *BMC ophthalmology*, *20*(1), 196. https://doi.org/10.1186/s12886-020-01467-0

Curcio, C. A., Medeiros, N. E., & Millican, C. L. (1996). Photoreceptor loss in age-related macular degeneration. *Investigative Ophthalmology and Visual Science*, *37*(7), 1236–1249.

Curcio, C. A., Owsley, C., & Jackson, G. R. (2000). Spare the rods, save the cones in aging and age-related maculopathy. *Investigative Ophthalmology and Visual Science*, *41*(8), 2015–2018.

Curcio, C. A., Zanzottera, E. C., Ach, T., Balaratnasingam, C., & Freund, K. B. (2017). Activated Retinal Pigment Epithelium, an Optical Coherence Tomography Biomarker for Progression in Age-Related Macular Degeneration. *Investigative ophthalmology & visual science*, *58*(6), BIO211–BIO226. https://doi.org/10.1167/iovs.17-21872

Dolz-Marco, R., Litts, K. M., Tan, A. C., Freund, K. B., & Curcio, C. A. (2017). The Evolution of Outer Retinal Tubulation, a Neurodegeneration and Gliosis Prominent in Macular Diseases. *Ophthalmology*, *124*(9), 1353–1367. https://doi.org/10.1016/j.ophtha.2017.03.043

Domalpally, A., Danis, R. P., White, J., Narkar, A., Clemons, T., Ferris, F., & Chew, E. (2013). Circularity index as a risk factor for progression of geographic atrophy. *Ophthalmology*, *120*(12), 2666–2671. https://doi.org/10.1016/j.ophtha.2013.07.047

Dysli, C., Wolf, S., Berezin, M. Y., Sauer, L., Hammer, M., & Zinkernagel, M. S. (2017). Fluorescence lifetime imaging ophthalmoscopy. *Progress in Retinal and Eye Research*, *60*, 120–143. https://doi.org/10.1016/j.preteyeres.2017.06.005

Dysli, C., Wolf, S., & Zinkernagel, M. S. (2016). Autofluorescence lifetimes in geographic atrophy in patients with age-related macular degeneration. *Inves-*

tigative Ophthalmology and Visual Science, *57*(6), 2479–2487. https://doi.org/10.1167/iovs.15-18381

Echols, B. S., Clark, M. E., Swain, T. A., Chen, L., Kar, D., Zhang, Y., Sloan, K. R., McGwin, G. J., Singireddy, R., Mays, C., Kilpatrick, D., Crosson, J. N., Owsley, C., & Curcio, C. A. (2020). Hyperreflective Foci and Specks Are Associated with Delayed Rod-Mediated Dark Adaptation in Nonneovascular Age-Related Macular Degeneration. *Ophthalmology. Retina*. https://doi.org/10.1016/j.oret.2020.05.001

Edwards, A. O., Ritter, R., Abel, K. J., Manning, A., Panhuysen, C., & Farrer, L. A. (2005). Complement factor H polymorphism and age-related macular degeneration. *Science*, *308*(5720), 421–424. https://doi.org/10.1126/science.1110189

Ferris, F. L., & Bailey, I. (1996). Standardizing the measurement of visual acuity for clinical research studies: Guidelines from the Eye Care Technology Forum. *Ophthalmology*, *103*(1), 181–182. https://doi.org/10.1016/S0161-6420(96)30742-2

Feuer, W. J., Yehoshua, Z., Gregori, G., Penha, F. M., Chew, E. Y., Ferris, F. L., Clemons, T. E., Lindblad, A. S., & Rosenfeld, P. J. (2013). Square root transformation of geographic atrophy area measurements to eliminate dependence of growth rates on baseline lesion measurements: A reanalysis of age-related eye disease study report no. 26. *Archives of Ophthalmology*, *131*(1), 110–111. https://doi.org/10.1001/jamaophthalmol.2013.572

Flamendorf, J., Agrón, E., Wong, W. T., Thompson, D., Wiley, H. E., Doss, E. L., Al-Holou, S., Ferris, F. L., Chew, E. Y., & Cukras, C. (2015). Impairments in dark adaptation are associated with age-related macular degeneration severity and reticular pseudodrusen. *Ophthalmology*, *122*(10), 2053–2062. https://doi.org/10.1016/j.ophtha.2015.06.023

Fleckenstein, M., Issa, P. C., Helb, H. M., Schmitz-Valckenberg, S., Finger, R. P., Scholl, H. P., Loeffler, K. U., & Holz, F. G. (2008). High-resolution spectral domain-OCT imaging in geographic atrophy associated with age-related macular degeneration. *Investigative Ophthalmology and Visual Science*, *49*(9), 4137–4144. https://doi.org/10.1167/iovs.08-1967

Fleckenstein, M., Mitchell, P., Freund, K. B., Sadda, S. V., Holz, F. G., Brittain, C., Henry, E. C., & Ferrara, D. (2018). The Progression of Geographic Atrophy Secondary to Age-Related Macular Degeneration. *Ophthalmology*, *125*(3), 369–390. https://doi.org/10.1016/j.ophtha.2017.08.038

Fleckenstein, M., Schmitz-Valckenberg, S., Adrion, C., Krämer, I., Eter, N., Helb, H. M., Brinkmann, C. K., Issa, P. C., Mansmann, U., & Holz, F. G. (2010). Tracking progression with spectral-domain optical coherence tomography in geographic atrophy caused by age-related macular degeneration. *Investigative Ophthalmology and Visual Science*, *51*(8), 3846–3852. https://doi.org/10.1167/iovs.09-4533

Flynn, O. J., Cukras, C. A., & Jeffrey, B. G. (2018). Characterization of rod function phenotypes across a range of age-related macular degeneration severities and subretinal drusenoid deposits. *Investigative Ophthalmology and Visual Science*, *59*(6), 2411–2421. https://doi.org/10.1167/iovs.17-22874

Fritsche, L. G., Fariss, R. N., Stambolian, D., Abecasis, G. R., Curcio, C. A., & Swaroop, A. (2014). Age-Related Macular Degeneration: Genetics and Biology Coming Together. *Annual Review of Genomics and Human Genetics*, *15*(1), 151–171. https://doi.org/10.1146/annurev-genom-090413-025610

Gliem, M., Hendig, D., Finger, R. P., Holz, F. G., & Issa, P. C. (2015). Reticular pseudodrusen associated with a diseased Bruch membranein pseudoxanthoma elasticum. *JAMA Ophthalmology*, *133*(5), 581–588. https://doi.org/10.1001/jamaophthalmol.2015.117

Gliem, M., Müller, P. L., Mangold, E., Bolz, H. J., Stöhr, H., Weber, B. H., Holz, F. G., & Charbel Issa, P. (2015). Reticular Pseudodrusen in Sorsby Fundus Dystrophy. *Ophthalmology*, *122*(8), 1555–1562. https://doi.org/10.1016/j.ophtha.2015.04.035

Grassmann, F., Fleckenstein, M., Chew, E. Y., Strunz, T., Schmitz-Valckenberg, S., Göbel, A. P., Klein, M. L., Ratnapriya, R., Swaroop, A., Holz, F. G., & Weber, B. H. (2015). Clinical and genetic factors associated with progression of geographic atrophy lesions in age-related macular degeneration. *PLoS ONE*, *10*(5), e0126636. https://doi.org/10.1371/journal.pone.0126636

Grassmann, F., Heid, I. M., & Weber, B. H. F. (2017). Recombinant Haplotypes Narrow the ARMS2/HTRA1 Association Signal for Age-Related Macular Degeneration. *Genetics*, *205*(2), 919–924. https://doi.org/10.1534/genetics.116.195966

Guymer, R. H., Markey, C. M., McAllister, I. L., Gillies, M. C., Hunyor, A. P., Arnold, J. J., Chang, A., Syed, A., Broadhead, G., Pham, T., Hong, T., Wong, L., Zhu, M., Burnett, S., Joachim, N., Wijeyakumar, W., Manalang, G., Mhlanga, C., Joachim, N., … Khalil, Z. (2019). Tolerating Subretinal Fluid in Neovascular Age-Related Macular Degeneration Treated with Ranibizumab Using a Treat-and-Extend Regimen: FLUID Study 24-Month Results. *Ophthalmology*, *126*(5), 723–734. https://doi.org/10.1016/j.ophtha.2018.11.025

Hageman, G. S., Anderson, D. H., Johnson, L. V., Hancox, L. S., Taiber, A. J., Hardisty, L. I., Hageman, J. L., Stockman, H. A., Borchardt, J. D., Gehrs, K. M., Smith, R. J., Silvestri, G., Russell, S. R., Klaver, C. C., Barbazetto, I., Chang, S., Yannuzzi, L. A., Barile, G. R., Merriam, J. C., … Allikmets, R. (2005). A common haplotype in the complement regulatory gene factor H (HF1/CFH) predisposes individuals to age-related macular degeneration. *Proceedings of the National Academy of Sciences of the United States of America*, *102*(20), 7227–7232. https://doi.org/10.1073/pnas.0501536102

Haines, J. L., Hauser, M. A., Schmidt, S., Scott, W. K., Olson, L. M., Gallins, P., Spencer, K. L., Shu, Y. K., Noureddine, M., Gilbert, J. R., Schnetz-Boutaud, N., Agarwal, A., Postel, E. A., & Pericak-Vance, M. A. (2005). Complement

factor H variant increases the risk of age-related macular degeneration. *Science*, *308*(5720), 419–421. https://doi.org/10.1126/science.1110359

Harmening, W. M., Tuten, W. S., Roorda, A., & Sincich, L. C. (2014). Mapping the perceptual grain of the human retina. *Journal of Neuroscience*, *34*(16), 5667–5677. https://doi.org/10.1523/JNEUROSCI.5191-13.2014

Heier, J. S., Pieramici, D., Chakravarthy, U., Patel, S. S., Gupta, S., Lotery, A., Lad, E. M., Silverman, D., Henry, E. C., Anderesi, M., Tschosik, E. A., Gray, S., Ferrara, D., & Guymer, R. (2020). Visual Function Decline Resulting from Geographic Atrophy: Results from the Chroma and Spectri Phase 3 Trials. *Ophthalmology Retina*, *4*(7), 673–688. https://doi.org/10.1016/j.oret.2020.01.019

Hess, K., Gliem, M., Birtel, J., Müller, P., Hendig, D., Andrews, C., Murray, I. J., Holz, F. G., & Charbel Issa, P. (2019). Impaired Dark Adaptation Associated With a Diseased Bruch Membrane in Pseudoxanthoma Elasticum. *Retina*, 1. https://doi.org/10.1097/iae.0000000000002689

Hess, K., Gliem, M., Charbel Issa, P., Birtel, J., Müller, P. L., von der Emde, L., Herrmann, P., Holz, F. G., & Pfau, M. (2020). Mesopic and Scotopic Light Sensitivity and Its Microstructural Correlates in Pseudoxanthoma Elasticum. *JAMA ophthalmology*. https://doi.org/10.1001/jamaophthalmol.2020.4335

Holz, F. G., Bindewald-Wittich, A., Fleckenstein, M., Dreyhaupt, J., Scholl, H. P., & Schmitz-Valckenberg, S. (2007). Progression of Geographic Atrophy and Impact of Fundus Autofluorescence Patterns in Age-related Macular Degeneration. *American Journal of Ophthalmology*, *143*(3), 463–72. https://doi.org/10.1016/j.ajo.2006.11.041

International Conference on Harmonisation E9 Expert Working Group. (1999). ICH Harmonised Tripartite Guideline. Statistical principles for clinical trials. International Conference on Harmonisation E9 Expert Working Group. *Statistics in medicine*, *18*(15), 1905–42. http://www.ncbi.nlm.nih.gov/pubmed/10532877

Jackson, G. R., Owsley, C., & McGwin, G. (1999). Aging and dark adaptation. *Vision Research*, *39*(23), 3975–3982. https://doi.org/10.1016/S0042-6989(99)00092-9

Jacobson, S. G., Aleman, T. S., Cideciyan, A. V., Sumaroka, A., Schwartz, S. B., Windsor, E. A., Traboulsi, E. I., Heon, E., Pittler, S. J., Milam, A. H., Maguire, A. M., Palczewski, K., Stone, E. M., & Bennett, J. (2005). Identifying photoreceptors in blind eyes caused by RPE65 mutations: Prerequisite for human gene therapy success. *Proceedings of the National Academy of Sciences of the United States of America*, *102*(17), 6177–6182. https://doi.org/10.1073/pnas.0500646102

Jacobson, S., Apathy, P., & Parel, J. (1991). Rod and cone perimetry: computerized testing and analysis (J. R. Heckenlively & G. Arden, Eds.). In J. R. Hecken-

lively & G. Arden (Eds.), *Principles and practice of clinical electrophysiology of vision*. Mosby-Year Book, Inc.

Jakobsdottir, J., Conley, Y. P., Weeks, D. E., Mah, T. S., Ferrell, R. E., & Gorin, M. B. (2005). Susceptibility genes for age-related maculopathy on chromosome 10q26. *American Journal of Human Genetics*, *77*(3), 389–407. https://doi.org/10.1086/444437

Johnson, P. T., Lewis, G. P., Talaga, K. C., Brown, M. N., Kappel, P. J., Fisher, S. K., Anderson, D. H., & Johnson, L. V. (2003). Drusen-associated degeneration in the retina. *Investigative Ophthalmology and Visual Science*, *44*(10), 4481–4488. https://doi.org/10.1167/iovs.03-0436

Kassoff, A., Kassoff, J., Buehler, J., Eglow, M., Kaufman, F., Mehu, M., Kieval, S., Mairs, M., Graig, B., Quattrocchi, A., Jones, D., Locatelli, J., Ruby, A., Capone A., J., Garretson, B., Hassan, T., Trese, M. T., Williams, G. A., Regan, V., ... Crouse, V. D. (2001). A randomized, placebo-controlled, clinical trial of high-dose supplementation with vitamins c and e and beta carotene for age-related cataract and vision loss: AREDS report no. 9. *Archives of Ophthalmology*, *119*(10), 1439–1452. https://doi.org/10.1001/archopht.119.10.1439

Keenan, T. D., Toso, M., Pappas, C., Nichols, L., Bishop, P. N., & Hageman, G. S. (2015). Assessment of proteins associated with complement activation and inflammation in maculae of human donors homozygous risk at chromosome 1 CFH-to-F13B. *Investigative Ophthalmology and Visual Science*, *56*(8), 4870–4879. https://doi.org/10.1167/iovs.15-17009

Kihara, Y., Heeren, T. F., Lee, C. S., Wu, Y., Xiao, S., Tzaridis, S., Holz, F. G., Charbel Issa, P., Egan, C. A., & Lee, A. Y. (2019). Estimating Retinal Sensitivity Using Optical Coherence Tomography With Deep-Learning Algorithms in Macular Telangiectasia Type 2. *JAMA network open*, *2*(2), e188029. https://doi.org/10.1001/jamanetworkopen.2018.8029

Klein, M. L., Ferris, F. L. 3., Armstrong, J., Hwang, T. S., Chew, E. Y., Bressler, S. B., & Chandra, S. R. (2008). Retinal precursors and the development of geographic atrophy in age-related macular degeneration. *Ophthalmology*, *115*(6), 1026–1031. https://doi.org/10.1016/j.ophtha.2007.08.030

Klein, R. J., Zeiss, C., Chew, E. Y., Tsai, J. Y., Sackler, R. S., Haynes, C., Henning, A. K., SanGiovanni, J. P., Mane, S. M., Mayne, S. T., Bracken, M. B., Ferris, F. L., Ott, J., Barnstable, C., & Hoh, J. (2005). Complement factor H polymorphism in age-related macular degeneration. *Science*, *308*(5720), 385–389. https://doi.org/10.1126/science.1109557

Klein, R., Klein, B. E. K., Knudtson, M. D., Wong, T. Y., Cotch, M. F., Liu, K., Burke, G., Saad, M. F., & Jacobs, D. R. J. (2006). Prevalence of age-related macular degeneration in 4 racial/ethnic groups in the multi-ethnic study of atherosclerosis. *Ophthalmology*, *113*(3), 373–380. https://doi.org/10.1016/j.ophtha.2005.12.013

Klein, R., Klein, B. E. K., Tomany, S. C., & Cruickshanks, K. J. (2003). The association of cardiovascular disease with the long-term incidence of age-related maculopathy: the Beaver Dam Eye Study. *Ophthalmology*, *110*(6), 1273–1280. https://doi.org/10.1016/S0161-6420(03)00599-2

Lamb, T. D., & Pugh, E. N. (2004). Dark adaptation and the retinoid cycle of vision. *Progress in Retinal and Eye Research*, *23*(3), 307–380. https://doi.org/10.1016/j.preteyeres.2004.03.001

Li, M., Dolz-Marco, R., Messinger, J. D., Sloan, K. R., Ferrara, D., Curcio, C. A., & Freund, K. B. (2019). Clinicopathologic Correlation of Aneurysmal Type 1 Neovascularization in Age-Related Macular Degeneration. *Ophthalmology Retina*, *3*(2), 99–111. https://doi.org/10.1016/j.oret.2018.08.008

Li, M., Huisingh, C., Messinger, J., Dolz-Marco, R., Ferrara, D., Bailey Freund, K., & Curcio, C. A. (2018). Histology of geographic atrophy secondary to age-related macular degeneration a multilayer approach. *Retina*, *38*(10), 1937–1953. https://doi.org/10.1097/IAE.0000000000002182

Lim, L. S., Mitchell, P., Seddon, J. M., Holz, F. G., & Wong, T. Y. (2012). Age-related macular degeneration. *The Lancet*, *379*(9827), 1728–1738. https://doi.org/10.1016/S0140-6736(12)60282-7

Lindner, M., Böker, A., Mauschitz, M. M., Göbel, A. P., Fimmers, R., Brinkmann, C. K., Schmitz-Valckenberg, S., Schmid, M., Holz, F. G., & Fleckenstein, M. (2015). Directional Kinetics of Geographic Atrophy Progression in Age-Related Macular Degeneration with Foveal Sparing. *Ophthalmology*, *122*(7), 1356–1365. https://doi.org/10.1016/j.ophtha.2015.03.027

Lindner, M., Pfau, M., Czauderna, J., Goerdt, L., Schmitz-Valckenberg, S., Holz, F. G., & Fleckenstein, M. (2019). Determinants of Reading Performance in Eyes with Foveal-Sparing Geographic Atrophy. *Ophthalmology Retina*, *3*(3), 201–210. https://doi.org/10.1016/j.oret.2018.11.005

Machida, S., Kondo, M., Jamison, J. A., Khan, N. W., Kononen, L. T., Sugawara, T., Bush, R. A., & Sieving, P. A. (2000). P23H rhodopsin transgenic rat: Correlation of retinal function with histopathology. *Investigative Ophthalmology and Visual Science*, *41*(10), 3200–3209.

McGuinness, M. B., Le, J., Mitchell, P., Gopinath, B., Cerin, E., Saksens, N. T., Schick, T., Hoyng, C. B., Guymer, R. H., & Finger, R. P. (2017). Physical Activity and Age-related Macular Degeneration: A Systematic Literature Review and Meta-analysis. *American Journal of Ophthalmology*, *180*, 29–38. https://doi.org/10.1016/j.ajo.2017.05.016

Meleth, A. D., Mettu, P., Agrón, E., Chew, E. Y., Sadda, S. R., Ferris, F. L., & Wong, W. T. (2011). Changes in retinal sensitivity in geographic atrophy progression as measured by microperimetry. *Investigative Ophthalmology and Visual Science*, *52*(2), 1119–1126. https://doi.org/10.1167/iovs.10-6075

Menon, M., Mohammadi, S., Davila-Velderrain, J., Goods, B. A., Cadwell, T. D., Xing, Y., Stemmer-Rachamimov, A., Shalek, A. K., Love, J. C., Kellis, M., & Hafler, B. P. (2019). Single-cell transcriptomic atlas of the human retina identifies cell types associated with age-related macular degeneration. *Nature Communications*, *10*(1), 4902. https://doi.org/10.1038/s41467-019-12780-8

Merle, B. M. J., Colijn, J. M., Cougnard-Grégoire, A., de Koning-Backus, A. P. M., Delyfer, M.-N., Kiefte-de Jong, J. C., Meester-Smoor, M., Féart, C., Verzijden, T., Samieri, C., Franco, O. H., Korobelnik, J.-F., Klaver, C. C. W., & Delcourt, C. (2019). Mediterranean Diet and Incidence of Advanced Age-Related Macular Degeneration: The EYE-RISK Consortium. *Ophthalmology*, *126*(3), 381–390. https://doi.org/10.1016/j.ophtha.2018.08.006

Müller, P. L., Pfau, M., Möller, P. T., Nadal, J., Schmid, M., Lindner, M., de Sisternes, L., Stöhr, H., Weber, B. H., Neuhaus, C., Herrmann, P., Schmitz-Valckenberg, S., Holz, F. G., & Fleckenstein, M. (2018). Choroidal flow signal in late-onset stargardt disease and age-related macular degeneration: An OCT-angiography study. *Investigative Ophthalmology and Visual Science*, *59*(4), AMD122–AMD131. https://doi.org/10.1167/iovs.18-23819

Müller, P. L., Pfau, M., Treis, T., Pascual-Camps, I., Birtel, J., Lindner, M., Herrmann, P., & Holz, F. G. (2020). Progression of Abca4-Related Retinopathy—Prognostic Value of Demographic, Functional, Genetic, and Imaging Parameters. *Retina*, 1. https://doi.org/10.1097/iae.0000000000002747

Müller, P. L., Treis, T., Pfau, M., Esposti, S. D., Alsaedi, A., Maloca, P., Balaskas, K., Webster, A., Egan, C., & Tufail, A. (2020). Progression of Retinopathy Secondary to Maternally Inherited Diabetes and Deafness – Evaluation of Predicting Parameters. *American Journal of Ophthalmology*, *213*, 134–144. https://doi.org/10.1016/j.ajo.2020.01.013

Mullins, R. F., Schoo, D. P., Sohn, E. H., Flamme-Wiese, M. J., Workamelahu, G., Johnston, R. M., Wang, K., Tucker, B. A., & Stone, E. M. (2014). The membrane attack complex in aging human choriocapillaris: Relationship to macular degeneration and choroidal thinning (2014/09/07). *American Journal of Pathology*, *184*(11), 3142–3153. https://doi.org/10.1016/j.ajpath.2014.07.017

Nassisi, M., Shi, Y., Fan, W., Borrelli, E., Uji, A., Ip, M. S., & Sadda, S. R. (2019). Choriocapillaris impairment around the atrophic lesions in patients with geographic atrophy: A swept-source optical coherence tomography angiography study. *British Journal of Ophthalmology*, *103*(7), 911–917. https://doi.org/10.1136/bjophthalmol-2018-312643

Neely, D., Zarubina, A. V., Clark, M. E., Huisingh, C. E., Jackson, G. R., Zhang, Y., McGwin, G., Curcio, C. A., & Owsley, C. (2017). Association Between Visual Function And Subretinal Drusenoid Deposits In Normal And Early Age-related Macular Degeneration Eyes. *Retina*, *37*(7), 1329–1336. https://doi.org/10.1097/IAE.0000000000001454

Niu, S., de Sisternes, L., Chen, Q., Rubin, D. L., & Leng, T. (2016). Fully Automated Prediction of Geographic Atrophy Growth Using Quantitative Spectral-Domain

Optical Coherence Tomography Biomarkers. *Ophthalmology*, *123*(8), 1737–1750. https://doi.org/10.1016/j.ophtha.2016.04.042

Olsson, J., Bengtsson, B., Heijl, A., & Rootzén, H. (1997). An improved method to estimate frequency of false positive answers in computerized perimetry. *Acta Ophthalmologica Scandinavica*, *75*(2), 181–183. https://doi.org/10.1111/j.1600-0420.1997.tb00120.x

Owsley, C., Jackson, G. R., Cideciyan, A. V., Huang, Y., Fine, S. L., Ho, A. C., Maguire, M. G., Lolley, V., & Jacobson, S. G. (2000). Psychophysical evidence for rod vulnerability in age-related macular degeneration. *Investigative Ophthalmology and Visual Science*, *41*(1), 267–273.

Owsley, C., McGwin, G., Clark, M. E., Jackson, G. R., Callahan, M. A., Kline, L. B., Witherspoon, C. D., & Curcio, C. A. (2016). Delayed Rod-Mediated Dark Adaptation Is a Functional Biomarker for Incident Early Age-Related Macular Degeneration. *Ophthalmology*, *123*(2), 344–351. https://doi.org/10.1016/j.ophtha.2015.09.041

Owsley, C., McGwin, G., Jackson, G. R., Heimburger, D. C., Piyathilake, C. J., Klein, R., White, M. F., & Kallies, K. (2006). Effect of short-term, high-dose retinol on dark adaptation in aging and early age-related maculopathy. *Investigative Ophthalmology and Visual Science*, *47*(4), 1310–1318. https://doi.org/10.1167/iovs.05-1292

Owsley, C., McGwin, G., Jackson, G. R., Kallies, K., & Clark, M. (2007). Cone- and Rod-Mediated Dark Adaptation Impairment in Age-Related Maculopathy. *Ophthalmology*, *114*(9), 1728–1735. https://doi.org/10.1016/j.ophtha.2006.12.023

Pauleikhoff, D., Harper, C. A., Marshall, J., & Bird, A. C. (1990). Aging Changes in Bruch's Membrane: A Histochemical and Morphologic Study. *Ophthalmology*, *97*(2), 171–178. https://doi.org/10.1016/S0161-6420(90)32619-2

Pfau, M., Goerdt, L., Schmitz-Valckenberg, S., Mauschitz, M. M., Mishra, D. K., Holz, F. G., Lindner, M., & Fleckenstein, M. (2017). Green-Light Autofluorescence Versus Combined Blue-Light Autofluorescence and Near-Infrared Reflectance Imaging in Geographic Atrophy Secondary to Age-Related Macular Degeneration. *Investigative ophthalmology & visual science*, *58*(6), BIO121–BIO130. https://doi.org/10.1167/iovs.17-21764

Pfau, M., Jolly, J. K., Wu, Z., Denniss, J., Lad, E. M., Guymer, R. H., Fleckenstein, M., Holz, F. G., & Schmitz-Valckenberg, S. (2020). Fundus-controlled perimetry (microperimetry): Application as outcome measure in clinical trials. *Progress in Retinal and Eye Research*, 100907. https://doi.org/https://doi.org/10.1016/j.preteyeres.2020.100907

Pfau, M., Lindner, M., Gliem, M., Steinberg, J. S., Thiele, S., Finger, R. P., Fleckenstein, M., Holz, F. G., & Schmitz-Valckenberg, S. (2018). Mesopic and dark-adapted two-color fundus-controlled perimetry in patients with cuticu-

lar, reticular, and soft drusen. *Eye (Basingstoke)*, *32*(12), 1819–1830. https://doi.org/10.1038/s41433-018-0183-3

Pfau, M., Müller, P. L., Von Der Emde, L., Lindner, M., Möller, P. T., Fleckenstein, M., Holz, F. G., & Schmitz-Valckenberg, S. (2020). Mesopic And Dark-adapted Two-color Fundus-controlled Perimetry In Geographic Atrophy Secondary To Age-related Macular Degeneration. *Retina*, *40*(1), 169–180. https://doi.org/10.1097/IAE.0000000000002337

Pfau, M., von der Emde, L., de Sisternes, L., Hallak, J. A., Leng, T., Schmitz-Valckenberg, S., Holz, F. G., Fleckenstein, M., & Rubin, D. L. (2020). Progression of Photoreceptor Degeneration in Geographic Atrophy Secondary to Age-related Macular Degeneration. *JAMA ophthalmology*. https://doi.org/10.1001/jamaophthalmol.2020.2914

Querques, G., Srour, M., Massamba, N., Georges, A., Ben Moussa, N., Rafaeli, O., & Souied, E. H. (2013). Functional characterization and multimodal imaging of treatment-naive "quiescent" choroidal neovascularization. *Investigative ophthalmology & visual science*, *54*(10), 6886–6892. https://doi.org/10.1167/iovs.13-11665

R Development Core Team 3.0.1. (2013). A Language and Environment for Statistical Computing. *Vienna, Austria*, ISBN 3-900051-07-0. http://www.r-project.org

Rivera, A., Fisher, S. A., Fritsche, L. G., Keilhauer, C. N., Lichtner, P., Meitinger, T., & Weber, B. H. (2005). Hypothetical LOC387715 is a second major susceptibility gene for age-related macular degeneration, contributing independently of complement factor H to disease risk. *Human Molecular Genetics*, *14*(21), 3227–3236. https://doi.org/10.1093/hmg/ddi353

Rofagha, S., Bhisitkul, R. B., Boyer, D. S., Sadda, S. R., & Zhang, K. (2013). Seven-year outcomes in ranibizumab-treated patients in ANCHOR, MARINA, and HORIZON: A multicenter cohort study (SEVEN-UP). *Ophthalmology*, *120*(11), 2292–2299. https://doi.org/10.1016/j.ophtha.2013.03.046

Roisman, L., Zhang, Q., Wang, R. K., Gregori, G., Zhang, A., Chen, C. L., Durbin, M. K., An, L., Stetson, P. F., Robbins, G., Miller, A., Zheng, F., & Rosenfeld, P. J. (2016). Optical Coherence Tomography Angiography of Asymptomatic Neovascularization in Intermediate Age-Related Macular Degeneration. *Ophthalmology*, *123*(6), 1309–1319. https://doi.org/10.1016/j.ophtha.2016.01.044

Rosenfeld, P. J., Brown, D. M., Heier, J. S., Boyer, D. S., Kaiser, P. K., Chung, C. Y., & Kim, R. Y. (2006). Ranibizumab for neovascular age-related macular degeneration. *New England Journal of Medicine*, *355*(14), 1419–1431. https://doi.org/10.1056/NEJMoa054481

Sadda, S. R., Guymer, R., Holz, F. G., Schmitz-Valckenberg, S., Curcio, C. A., Bird, A. C., Blodi, B. A., Bottoni, F., Chakravarthy, U., Chew, E. Y., Csaky, K., Danis, R. P., Fleckenstein, M., Freund, K. B., Grunwald, J., Hoyng, C. B.,

Jaffe, G. J., Liakopoulos, S., Monés, J. M., … Staurenghi, G. (2018). Consensus Definition for Atrophy Associated with Age-Related Macular Degeneration on OCT: Classification of Atrophy Report 3. *Ophthalmology*, *125*(4), 537–548. https://doi.org/10.1016/j.ophtha.2017.09.028

Sadigh, S., Cideciyan, A. V., Sumaroka, A., Huang, W. C., Luo, X., Swider, M., Steinberg, J. D., Stambolian, D., & Jacobson, S. G. (2013). Abnormal thickening as well as thinning of the photoreceptor layer in intermediate age-related macular degeneration. *Investigative Ophthalmology and Visual Science*, *54*(3), 1603–1612. https://doi.org/10.1167/iovs.12-11286

Sarks, J. P., Sarks, S. H., & Killingsworth, M. C. (1988). Evolution of geographic atrophy of the retinal pigment epithelium. *Eye*, *2*(5), 552–577. https://doi.org/10.1038/eye.1988.106

Sarks, S. H. (1976). Ageing and degeneration in the macular region: A clinico-pathological study. *British Journal of Ophthalmology*, *60*(5), 324–341. https://doi.org/10.1136/bjo.60.5.324

Schmitz-Valckenberg, S., Brinkmann, C. K., Alten, F., Herrmann, P., Stratmann, N. K., Göbel, A. P., Fleckenstein, M., Diller, M., Jaffe, G. J., & Holz, F. G. (2011). Semiautomated image processing method for identification and quantification of geographic atrophy in age-related macular degeneration. *Investigative Ophthalmology and Visual Science*, *52*(10), 7640–7646. https://doi.org/10.1167/iovs.11-7457

Schmitz-Valckenberg, S., Fleckenstein, M., Göbel, A. P., Hohman, T. C., & Holz, F. G. (2011). Optical coherence tomography and autofluorescence findings in areas with geographic atrophy due to age-related macular degeneration. *Investigative Ophthalmology and Visual Science*, *52*(1), 1–6. https://doi.org/10.1167/iovs.10-5619

Schmitz-Valckenberg, S., Sahel, J. A., Danis, R., Fleckenstein, M., Jaffe, G. J., Wolf, S., Pruente, C., & Holz, F. G. (2016). Natural History of Geographic Atrophy Progression Secondary to Age-Related Macular Degeneration (Geographic Atrophy Progression Study). *Ophthalmology*, *123*(2), 361–368. https://doi.org/10.1016/j.ophtha.2015.09.036

Shelley, E. J., Madigan, M. C., Natoli, R., Penfold, P. L., & Provis, J. M. (2009). Cone degeneration in aging and age-related macular degeneration. *Archives of Ophthalmology*, *127*(4), 483–492. https://doi.org/10.1001/archophthalmol.2008.622

Shen, L., Liu, F., Grossetta Nardini, H., & Del Priore, L. V. (2018). Natural History of Geographic Atrophy in Untreated Eyes with Nonexudative Age-Related Macular Degeneration: A Systematic Review and Meta-analysis. *Ophthalmology Retina*, *2*(9), 914–921. https://doi.org/10.1016/j.oret.2018.01.019

Sleiman, K., Veerappan, M., Winter, K. P., McCall, M. N., Yiu, G., Farsiu, S., Chew, E. Y., Clemons, T., Toth, C. A., Toth, C. A., Wong, W., Huang, T., Hubbard, G. B., Srivastava, S., McCall, M., Winter, K., Sarin, N., Hall, K.,

McCollum, P., ... Chew, E. (2017). Optical Coherence Tomography Predictors of Risk for Progression to Non-Neovascular Atrophic Age-Related Macular Degeneration (2017/08/26). *Ophthalmology*, *124*(12), 1764–1777. https://doi.org/10.1016/j.ophtha.2017.06.032

Smith, W., Assink, J., Klein, R., Mitchell, P., Klaver, C. C., Klein, B. E., Hofman, A., Jensen, S., Wang, J. J., & De Jong, P. T. (2001). Risk factors for age-related macular degeneration: Pooled findings from three continents. *Ophthalmology*, *108*(4), 697–704. https://doi.org/10.1016/S0161-6420(00)00580-7

Spaide, R. F., Jaffe, G. J., Sarraf, D., Freund, K. B., Sadda, S. R., Staurenghi, G., Waheed, N. K., Chakravarthy, U., Rosenfeld, P. J., Holz, F. G., Souied, E. H., Cohen, S. Y., Querques, G., Ohno-Matsui, K., Boyer, D., Gaudric, A., Blodi, B., Baumal, C. R., Li, X., ... Fujimoto, J. (2020). Consensus Nomenclature for Reporting Neovascular Age-Related Macular Degeneration Data: Consensus on Neovascular Age-Related Macular Degeneration Nomenclature Study Group. *Ophthalmology*, *127*(5). https://doi.org/10.1016/j.ophtha.2019.11.004

Steinberg, J. S., Auge, J., Jaffe, G. J., Fleckenstein, M., Holz, F. G., & Schmitz-Valckenberg, S. (2013). Longitudinal analysis of reticular drusen associated with geographic atrophy in age-related macular degeneration. *Investigative Ophthalmology and Visual Science*, *54*(6), 4054–4060. https://doi.org/10.1167/iovs.12-11538

Steinberg, J. S., Fitzke, F. W., Fimmers, R., Fleckenstein, M., Holz, F. G., & Schmitz-Valckenberg, S. (2015). Scotopic and photopic microperimetry in patients with reticular drusen and age-related macular degeneration. *JAMA Ophthalmology*, *133*(6), 690–697. https://doi.org/10.1001/jamaophthalmol.2015.0477

Steinberg, J. S., Saßmannshausen, M., Fleckenstein, M., Fimmers, R., Oishi, A., Holz, F. G., & Schmitz-Valckenberg, S. (2016). Correlation of Partial Outer Retinal Thickness with Scotopic and Mesopic Fundus-Controlled Perimetry in Patients with Reticular Drusen. *American Journal of Ophthalmology*, *168*, 52–61. https://doi.org/10.1016/j.ajo.2016.04.025

Sumaroka, A., Garafalo, A. V., Semenov, E. P., Sheplock, R., Krishnan, A. K., Roman, A. J., Jacobson, S. G., & Cideciyan, A. V. (2019). Treatment potential for macular cone vision in leber congenital amaurosis due to CEP290 or NPHP5 mutations: Predictions from artificial intelligence. *Investigative Ophthalmology and Visual Science*, *60*(7), 2551–2562. https://doi.org/10.1167/iovs.19-27156

Sunness, J. S., Johnson, M. A., Massof, R. W., & Marcus, S. (1988). Retinal Sensitivity Over Drusen and Nondrusen Areas: A Study Using Fundus Perimetry. *Archives of Ophthalmology*, *106*(8), 1081–1084. https://doi.org/10.1001/archopht.1988.01060140237032

Sunness, J. S., Margalit, E., Srikumaran, D., Applegate, C. A., Tian, Y., Perry, D., Hawkins, B. S., Bressler, N. M., Margalit, E., Srikumaran, D., Apple-

gate, C. A., Tian, Y., Perry, D., Hawkins, B. S., & Bressler, N. M. (2007). The Long-term Natural History of Geographic Atrophy from Age-Related Macular Degeneration. Enlargement of Atrophy and Implications for Interventional Clinical Trials. *Ophthalmology*, *114*(2), 271–277. https://doi.org/10.1016/j.ophtha.2006.09.016

Sunness, J. S., Rubin, G. S., Broman, A., Applegate, C. A., Bressler, N. M., & Hawkins, B. S. (2008). Low Luminance Visual Dysfunction as a Predictor of Subsequent Visual Acuity Loss from Geographic Atrophy in Age-Related Macular Degeneration. *Ophthalmology*, *115*(9), 1480–8. https://doi.org/10.1016/j.ophtha.2008.03.009

Tan, R., Guymer, R. H., & Luu, C. D. (2018). Subretinal drusenoid deposits and the loss of rod function in intermediate age-related macular degeneration. *Investigative Ophthalmology and Visual Science*, *59*(10), 4154–4161. https://doi.org/10.1167/iovs.18-23970

Thulliez, M., Zhang, Q., Shi, Y., Zhou, H., Chu, Z., de Sisternes, L., Durbin, M. K., Feuer, W., Gregori, G., Wang, R. K., & Rosenfeld, P. J. (2019). Correlations between Choriocapillaris Flow Deficits around Geographic Atrophy and Enlargement Rates Based on Swept-Source OCT Imaging. *Ophthalmology Retina*, *3*(6), 478–488. https://doi.org/10.1016/j.oret.2019.01.024

Tom, I., Pham, V. C., Katschke, K. J., Li, W., Liang, W. C., Gutierrez, J., Young, A. A., Figueroa, I., Eshghi, S. T., Lee, C. W. V., Kanodia, J., Snipas, S. J., Salvesen, G. S., Lai, P., Honigberg, L., Van Lookeren Campagne, M., Kirchhofer, D., Baruch, A., & Lill, J. R. (2020). Development of a therapeutic anti-HtrA1 antibody and the identification of DKK3 as a pharmacodynamic biomarker in geographic atrophy. *Proceedings of the National Academy of Sciences of the United States of America*, *117*(18), 9952–9963. https://doi.org/10.1073/pnas.1917608117

von der Emde, L., Thiele, S., Pfau, M., Nadal, J., Meyer, J., Möller, P. T., Schmid, M., Fleckenstein, M., Holz, F. G., & Schmitz-Valckenberg, S. (2020). Assessment of Exudative Activity of Choroidal Neovascularization in Age-Related Macular Degeneration by OCT Angiography. *Ophthalmologica*, *243*(2), 120–128. https://doi.org/10.1159/000503609

von der Emde, L., Pfau, M., Dysli, C., Thiele, S., Möller, P. T., Lindner, M., Schmid, M., Fleckenstein, M., Holz, F. G., & Schmitz-Valckenberg, S. (2019). Artificial intelligence for morphology-based function prediction in neovascular age-related macular degeneration. *Scientific reports*, *9*(1), 11132. https://doi.org/10.1038/s41598-019-47565-y

Wang, J. S., & Kefalov, V. J. (2011). The Cone-specific visual cycle. *Progress in Retinal and Eye Research*, *30*(2), 115–128. https://doi.org/10.1016/j.preteyeres.2010.11.001

Wang, L., Li, C. M., Rudolf, M., Belyaeva, O. V., Chung, B. H., Messinger, J. D., Kedishvili, N. Y., & Curcio, C. A. (2009). Lipoprotein particles of intraocular origin in human bruch membrane: An unusual lipid profile. *Investigative*

Ophthalmology and Visual Science, *50*(2), 870–877. https://doi.org/10.1167/iovs.08-2376

Wong, W. L., Su, X., Li, X., Cheung, C. M. G., Klein, R., Cheng, C. Y., & Wong, T. Y. (2014). Global prevalence of age-related macular degeneration and disease burden projection for 2020 and 2040: A systematic review and meta-analysis. *The Lancet Global Health*, *2*(2). https://doi.org/10.1016/S2214-109X(13)70145-1

Zanzottera, E. C., Ach, T., Huisingh, C., Messinger, J. D., Freund, K. B., & Curcio, C. A. (2016). Visualizing retinal pigment epithelium phenotypes in the transition to atrophy in neovascular age-related macular degeneration. *Retina*, *36*, S26–S39. https://doi.org/10.1097/IAE.0000000000001330

Zweifel, S. A., Spaide, R. F., Curcio, C. A., Malek, G., & Imamura, Y. (2010). Reticular Pseudodrusen Are Subretinal Drusenoid Deposits. *Ophthalmology*, *117*(2), 303–12. https://doi.org/10.1016/j.ophtha.2009.07.014

Chapter 7

Acknowledgements

First and foremost, I express my deepest gratitude to Professor Frank G. Holz for his overarching support of my academic career, his generous encouragement and for fostering an ideal postgraduate research environment in Bonn. I profoundly appreciate Professor Monika Fleckenstein and Professor Steffen Schmitz-Valckenberg for their mentorship, the unique opportunity to work in the *'Directional Spread in Geographic Atrophy (DSGA)'* study group as well as the innumerable hours devoted to supervisory meetings, project-related discussions, editing of manuscripts and proofreading of grant proposals.

A grand thank you to Moritz Lindner for providing me with an extensive one-on-one introduction to the whole spectrum of skills ranging form hands-on imaging to manuscript writing. Many of our conversations were instrumental in defining the path of my research.

Likewise, I thank Joanna Czauderna, Verena Bonn and Ruth Hassenrik for patient coordination and data acquisition. I am grateful for the doctoral students of our group (in alphabetical order) Lukas Goerdt, Muriel Huss, Sandrine Künzel, and Leon von der Emde without whom it would not be possible to complete this work.

Special thanks are due to Professor Matthias Schmid and Jennifer Nadal for the support and guidance regarding the statistical analyses.

I am grateful for the support from many of my colleagues within my research group (Sarah Thiele, Marlene Saßmannshausen, Philipp Möller, Chantal Dysli) and from the other research groups (Philipp L. Müller, Kristina Hess, Maximilian W.M. Wintergerst, Matthias M. Mauschitz, Jan H. Terheyden, Petra P. Larsen) including all of the collaborative projects.

Moreover, I appreciate the research support and encouragement from Professor Matthias D. Becker, Professor Stephan Michels, Florentina Freiberg, Stephan Kinzl and Juliana Wons during my internship year. I am thankful for having had the opportunity to work as a short-term research fellow at the Doheny Eye Institute under the supervision of Professor SriniVas R. Sadda as well as Muneeswar Gupta Nittala and Privatdozentin Mayss Al-Sheikh.

Last, I thank all of my senior and junior colleagues in Bonn as well as outside of Bonn who have collaborated with me, or helped me with constructive feedback and meticulous comments, or advised me in various ways (in alphabetical order): Catherine A. Cukras, MD/PhD, Professor Christine A. Curcio, PhD, Jonathan Denniss,

PhD, Professor Robert P. Finger, Privatdozent Martin Gliem, Professor Robyn H. Guymer, Professor Joelle A. Hallak, Dr. rer. nat. Wolf M. Harmening, Dr. Tjebo F.C. Heeren, Professor Peter C. Issa, Brett Jeffrey, PhD, Jasleen K. Jolly, DPhil, Professor Theodore Leng, Professor Karin U. Löffler, Professor Cynthia Owsley, PhD, MSPH, Professor Daniel L. Rubin, Professor Gary S. Rubin, Luis de Sisternes, PhD, and Zichao Wu, PhD.

Chapter 8

Curriculum vitae

Maximilian Pfau
Schlossgasse 22, 74821 Mosbach, Germany
Maximilian.Pfau@ukbonn.de
+1 650 505 6799

EDUCATION

Heidelberg University, Germany, *Medicine* 10/2008 – 10/2015
Scholarship awardee of the German National Merit Foundation

Zurich Triemli Hospital, Switzerland, *Internship year, ophthalmology rotation* 09/2014 – 12/2014
Scholarship awardee of the German Academic Exchange Service

University of Eldoret, Kenya, *Surgery elective* 06/2012 – 08/2012

Karolinska Institute, Sweden, *Year abroad (anesthesia, surgery, ob-gyn, pediatrics)* 08/2011 – 05/2012
Scholarship awardee of the EU Erasmus program

RESEARCH EXPERIECNE

National Eye Institute, Bethesda, MD, *Postdoctoral scholar* 11/2020 – present
Supervisor: Brett G. Jeffrey, PhD, Catherine A. Cukras, MD, PhD
Funding: German Research Foundation

Dept. of Biomedical Data Science, Stanford University, CA, *Postdoctoral scholar* 08/2019 – 11/2020
Supervisor: Daniel L. Rubin, MD, MS
Funding: German Research Foundation

Dept. of Ophthalmology, University of Bonn, Germany, *Clinician scientist* 10/2015 – 07/2019
Supervisors: Dr. M. Fleckenstein, Dr. F.G. Holz, Dr. S. Schmitz-Valckenberg
Funding: German Research Foundation, University of Bonn

Doheny Eye Inst., University of California Los Angeles, CA, *Short-term research fellow* 07/2015 – 09/2015
Supervisor: Dr. SriniVas R. Sadda
Funding: German National Merit Foundation

Biochemistry Center, Heidelberg University, Germany, *Undergraduate research fellow, basic science doctoral thesis (Dr. med.) on SNARE mediated membrane fusion* 08/2012 – 06/2015
Supervisor: Professor Dr. T.H. Söllner

EMPLOYMENT AND CLINICAL APPOINTMENTS

Dept. of Ophthalmology, University of Bonn, Germany, *Ophthalmology resident* 11/2015 – present
Chairman: Dr. F.G. Holz

GRADE Reading Center, Bonn, Germany, *Grader and Senior Grader (since 07/2017)* 11/2015 – present

GRANTS

German Research Foundation (DFG) PF 950/1-1 08/2019 – present
„Deep-Learning-basierte Phänotypisierung und Vorhersage der Krankheitsprogression bei geographischer Atrophie infolge altersabhängiger Makuladegeneration“
Total: EUR 84,177.12
PI: M. Pfau

GRANTS (cont.)

BONFOR grant, University of Bonn, Instrument 2, O-137.0025.2 „Rapid Serial Visual Presentation in Macular Diseases: Development of an innovative approach for Low-Vision Rehabilitation utilizing state-of-the-art high-resolution retinal imaging and functional testing“ Total: EUR 91,000.00 PI: M. Pfau	08/2018 – 07/2019
BONFOR grant, University of Bonn, Instrument 2, O-137.0025 „Klinische Psychophysik und hochauflösende strukturelle Bildgebung bei geographischer Atrophie infolge altersabhängiger Makuladegeneration“ Total: EUR 47,100.00 PI: M. Pfau	07/2017 – 06/2018
BONFOR grant, University of Bonn, Instrument 6, O-137.0022 „Prädiktion und Charakterisierung der Progression retinaler Atrophie bei altersabhängiger Makuladegeneration“ Total: EUR 73,000.00 PI: M. Pfau	04/2016 – 03/2017

AWARDS AND HONORS

Young investigator award of the North Rhine-Westphalia Ophthalmological Society 2020 (EUR 20,000)	01.02.2020
Travel Grant of the German Retina Society (*Retinologische Gesellschaft*) 2019 (EUR 500)	29.06.2019
Clinical Investigator Award 2018 of the PRO RETINA foundation (EUR 2,000)	29.09.2018
EYEnovative 2018 Investigator Award funded by Novartis, Germany (EUR 25,000)	14.04.2018
BONFOR Investigator Award of the University of Bonn (EUR 400)	12.01.2018
“Dr.-Werner-Jackstädt” Young Investigator Award of the German Retina Society (*Retinologische Gesellschaft*) 2017 (EUR 10,000)	24.06.2017
International Travel Grant of the ARVO (*Association for Research in Vision and Ophthalmology*) for the annual meeting 2017 (USD 1,100)	07.05.2017
“Dr. Rolf M. Schwiete” foundation prize for the best German result in the Basic Science examination of the ICO (*International Council of Ophthalmology*) in 2016 (EUR 5,000)	01.10.2016
“Posters of the Day“ Annual Meeting 2016 of the German Ophthalmological Society DOG (*Deutsche ophthalmologische Gesellschaft*)	30.09.2016

Chapter 9

Declaration

Hiermit bestätige ich, dass ich die Richtlinien zur guten wissenschaftlichen Praxis der Universität Bonn, laut Habilitationsordnung, zur Kenntnis genommen habe und ich versichere, dass ich sie beim Verfassen der Habilitationsschrift beachtet habe. Insbesondere versichere ich, dass ich alle in der Habilitationsschrift benutzten Quellen und Hilfsmittel angegeben habe.